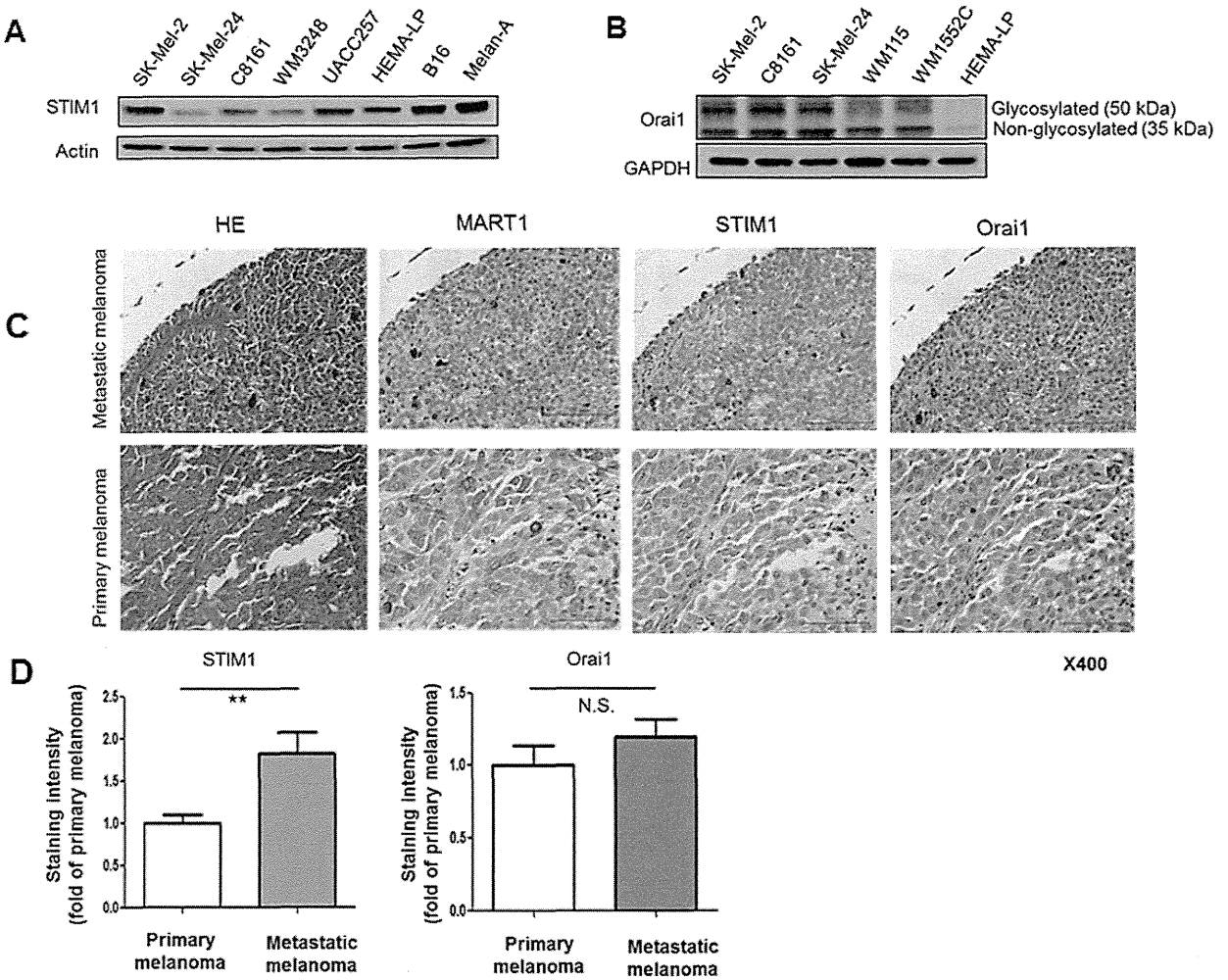

Figure 1. Expression of STIM1 and Orai1 in melanoma. (**A and B**) Western blot analyses of STIM1 (A) and Orai1 (B) expression in the indicated cell lines. (**C**) Immunohistochemical stainings of HE, MART1, STIM1 (the antibody from Abnova was used) and Orai1 (the antibody from Sigma was used) in a melanoma tissue microarray (original magnification, x400). Calibration bars represent 100 μm. (**D**) Analyses of the staining intensity of expression of STIM1 and Orai1. *, $p<0.05$; **, $p<0.01$, n = 8.
doi:10.1371/journal.pone.0089292.g001

Materials and Methods

Reagents and Cell Lines

Reagents were purchased from Sigma unless otherwise specified. Antibodies to β-actin, GAPDH, and ERK were purchased from Santa Cruz. α-Spectrin antibody was purchased from Millipore. Phospho-ERK antibody was purchased from Cell Signaling. Antibodies against STIM1 were purchased from BD Transduction Laboratories and Abnova [18]. Antibodies against Orai1 were previously generated by us [19], or purchased from Sigma [12]. Second antibodies for mouse and rabbit were purchased from Abcam and Cell Signaling, respectively. GW5074 was purchased from Focus Biomolecules. W5 hydrochloride was purchased from Tokyo Chemical Industry. GDC-0879 was purchased from Selleckhem [20]. SK-Mel-2 and SK-Mel-24 (human metastatic melanoma) cell lines were obtained from the American Type Culture Collection. UACC257 (human metastatic melanoma) was obtained from the Charles River Laboratory. Melan-A mouse melanocyte cell line was purchased from Welcome Trust Functional Genomics Cell Bank, St. George's, University of London. C8161 cell line was kindly provided by Dr. Mary J.C. Hendrix. WM3248 and WM115 (primary melanoma, vertical growth phase (VGP)) and WM1552C (primary melanoma, radial growth phase (RGP)) cell lines were kindly provided by Dr. Meenhard Herlyn. HEMA-LP (human melanocyte) cell line was obtained from Invitrogen. SK-Mel-2 and SK-Mel-24 cells were maintained in MEM containing 10% fetal bovine serum (FBS) and 1% penicillin-streptomycin. UACC257 cells were maintained in RPMI-1640 (Sigma) containing 10% FBS and 1% penicillin-streptomycin. HEMA-LP was maintained in an EndoGRO-VEGF Complete media kit (Millipore). All other melanoma cells were maintained in RPMI (Gibco) containing 10% FBS and 1% penicillin-streptomycin.

Western Blot Analysis

Western blot analyses were performed as we previously described [21]. Briefly, cells were lysed and sonicated in RIPA buffer (Thermo Scientific). Equal amounts of protein were subjected to sodium dodecyl sulfate polyacrylamide gel electro-

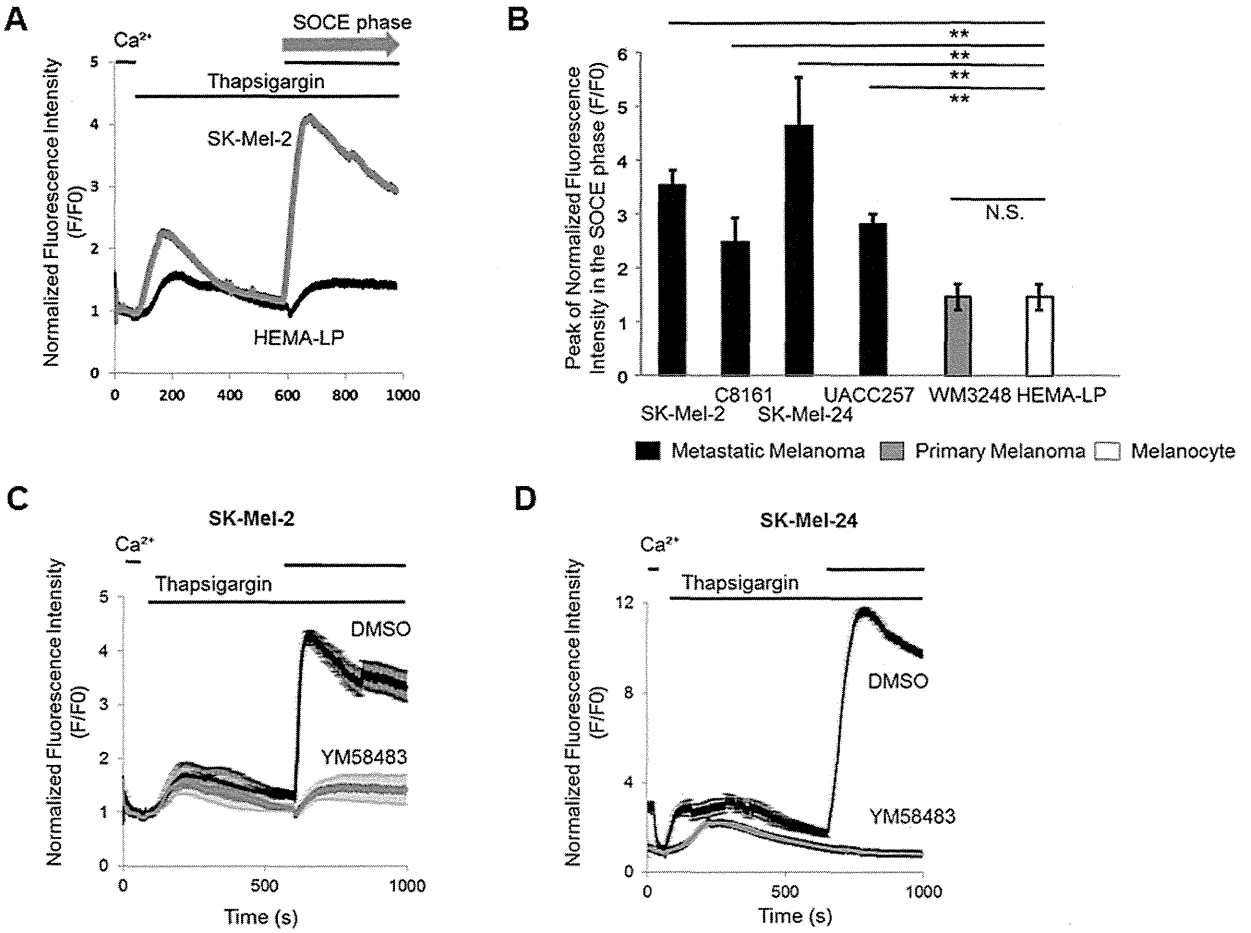

Figure 2. SOCE occurs in melanoma. (**A**) Cytosolic Ca^{2+} levels in SK-Mel-2 cells. Extracellular Ca^{2+} (2 mM) was removed, followed by the addition of thapsigargin (TG) (2 μM) for Ca^{2+} depletion in the ER. Ca^{2+} (2 mM) was then added to the extracellular fluid, and SOCE-induced Ca^{2+} elevation was observed (SOCE phase). (**B**) Ca^{2+} peak amplitude in the SOCE phase was compared among melanoma and melanocyte cell lines. **, $p<0.01$ (HEMA-LP), n = 6–8. (**C and D**) Cytosolic Ca^{2+} levels in SK-Mel-2 and SK-Mel-24 cells are shown as means ± SD (n = 6–10). SOCE was examined in the presence or absence of DMSO (1 μM) or YM58483 (1 μM) in SK-Mel-2 (**C**) and SK-Mel-24 cells (**D**).
doi:10.1371/journal.pone.0089292.g002

phoresis (SDS-PAGE). After protein separation by electrophoresis, samples were transferred to Millipore Immobilon-P membrane followed by immunoblotting with antibodies against molecules of interest. Immunoblottings for STIM1 and Orai1 were performed with the antibodies from BD Transduction Laboratories and from Sigma, respectively. Signal intensities of bands were quantified with Image J software (NIH).

Immunohistochemistry

Immunohistochemical stainings were performed as we previously described [22]. Melanoma tissue microarray plates (US Biomax Cat. #T085 and #ME1004a) were subjected to immunohistochemistry with antibodies against melanoma antigen recognized by T-cells 1 (MART1) (Millipore), STIM1 and Orai1. Two different antibodies against STIM1 (purchased from BD Transduction Laboratories and Abnova) and Orai1 (generated by us [19] and purchased from Sigma) were used to confirm the specificity of the staining. Negative control samples were exposed to the secondary antibody alone. Quantification of STIM1 expression was performed with BZ-II analyzer software (Keyence) as we previously described [23].

Fluorescence Imaging of Intracellular Ca^{2+}

Measurement of intracellular Ca^{2+} level was performed as we previously described [24]. Cells were incubated with 2-[4-(2-hydroxyethyl)-1-piperazinyl]ethanesulfonic acid (HEPES) buffer containing 4 μmol/l of Fluo-4AM, followed by washing and incubation with HEPES-buffered saline containing 2.0 mmol/L of $CaCl_2$. An iXon+885 charge-coupled-device camera (Andor Technology) was used to monitor fluorescence changes. Full images were collected every 4 s. Fluo-4 fluorescence was excited at 488 nm, and data were expressed as normalized changes in background-corrected fluorescence emission (F/F_0). Data were analyzed using Imaging Workbench (INDEC BioSystems). Representative Ca^{2+} signals averaged from 6 to 10 individual cells are shown in the figures.

Transduction of Short Hairpin RNA (shRNA)

SK-Mel-2, SK-Mel-24 and C8161 cells were transduced with STIM1 shRNA, Orai1 shRNA, and scramble control shRNA using lentivirus (Santa Cruz Biotechnology) according to the protocols provided by the manufacturer. Briefly, cells were incubated with 10 μg/mL of Polybrene (Santa Cruz Biotechnol-

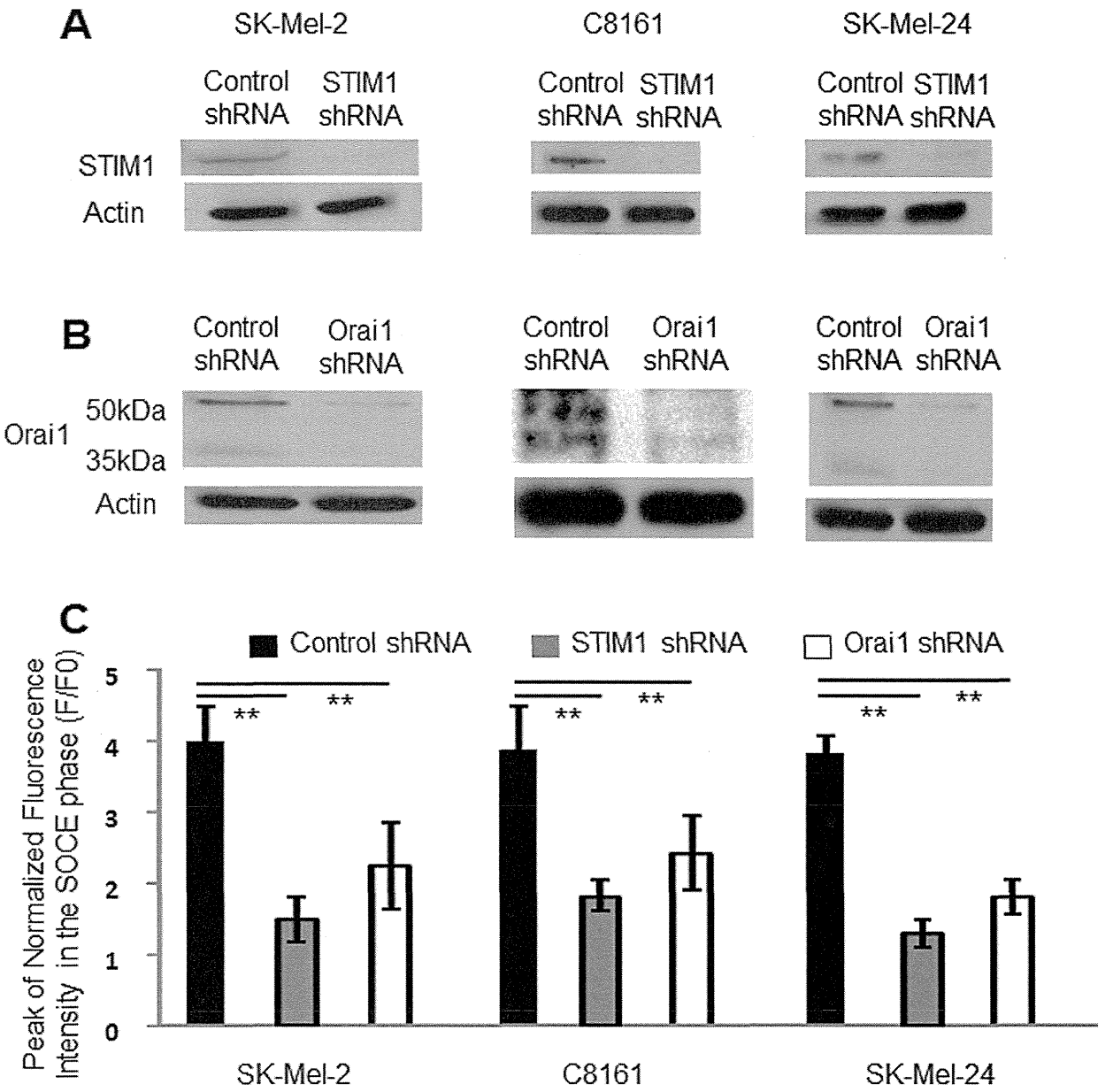

Figure 3. SOCE was inhibited by STIM1- or by Orai1-knockdown in melanoma cell lines. (**A and B**) Western blot analyses of protein expressions of STIM1 (A) and Orai1 (B) in metastatic melanoma cell lines. shRNA transduction reduced expression of the target proteins. (**C**) Ca^{2+} peak amplitude of SOCE was reduced by STIM1- or Orai1-knockdown. **, $p<0.01$, n = 6–10.
doi:10.1371/journal.pone.0089292.g003

ogy) and lentiviral particles harboring each shRNA, then selected with puromycin dihydrochloride (Santa Cruz Biotechnology) for 1 week. Puromycin-containing medium was replaced with fresh medium every 3 to 4 days.

3-(4,5-Dimethylthiazol-2-yl)-2,5-diphenyltetrazolium Bromide (MTT) Assay

Cells were seeded in a 96-well plate at 5,000 or 10,000 cells per well and cultured for 24 h. Viable cells were determined daily using the MTT Cell Proliferation Assay kit (ATCC) according to the manufacturer's instructions.

Apoptosis Assays

Apoptosis assays were performed as previously described [25]. Cells were seeded on 6 cm dishes, and incubated for 24 or 48 hours. Cells were washed twice with cold PBS, and transferred into culture tubes. Annexin V, allophycocyanin conjugate (APC) and 7-amino-actinomycin D (7-AAD) (BD Biosciences, California, U.S.A.) were then added to the tubes. Cells were incubated for 15 min at RT (25°C) in darkness, followed by FACS analysis (Canto^{TM} II, Japan Becton, Dickinson and Company, Tokyo, Japan) within 1 hour.

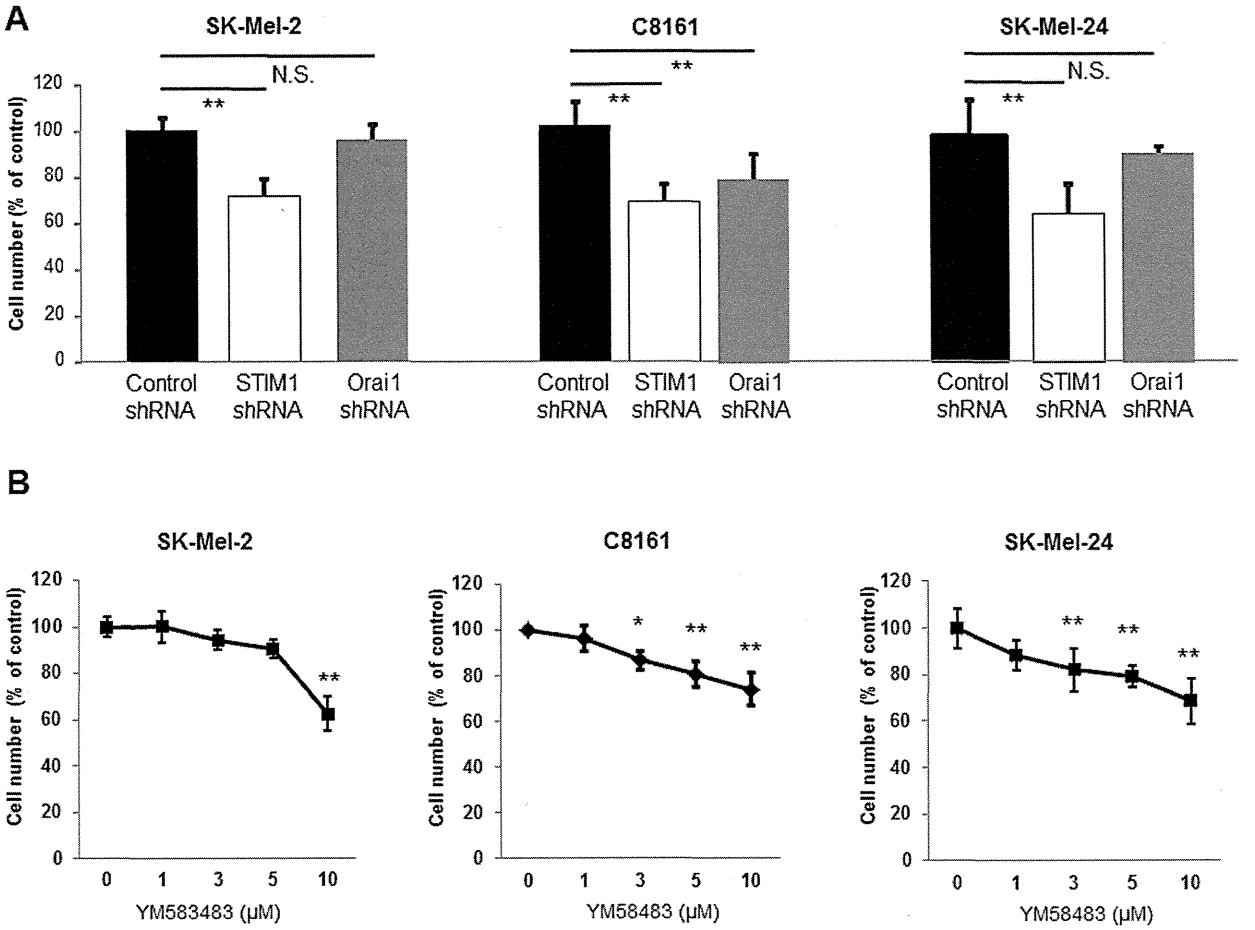

Figure 4. SOCE regulates proliferation of melanoma cells. (**A**) MTT assay of metastatic melanoma cell lines with or without STIM1- or Orai1-knockdown. **, $p<0.01$, n = 8. Representative data of 3 independent experiments are shown. (**B**) MTT assay of the indicated cell lines in the presence or absence of YM58483. *, $p<0.05$; **, $p<0.01$, n = 8. Representative data of 3 independent experiments are shown.
doi:10.1371/journal.pone.0089292.g004

Migration Assays

Migration assays were performed using 24-well Boyden chambers (8 μm pores, BD Biosciences) as we previously described [25]. The cells were plated at a density of 1×10^5 cells/100 μl of medium in the inserts, and incubated for 3 h at 37°C, followed by staining using a Diff-Quick kit (SIMENS). Pictures were taken with a microscope to count the number of migrated cells. The scratch wound method was also employed in some experiments as follows. Cells were seeded and allowed to form a monolayer for 24 h. The dish was scraped with the tip of a 100 μl pipette, and the resulting wound was washed with PBS two times [12]. Culture medium containing 10% FBS was added to the cells, and the cells were incubated at 37°C in 5% CO_2. Bright-field images were captured (Olympus IX51 microscope) and analyzed (Adobe Photoshop). The total number of pixels in empty spaces inside the wound were counted and normalized to the control.

Time-lapse Videomicroscopy

Analysis of cell motility using time-lapse videomicroscopy was performed as we previously described [25]. SK-Mel-2 cells were subjected to time-lapse video recording. Frames from the recording were digitized at 15-min intervals. Moving distance of each cell was analyzed by Image J software (NIH).

Calpain Activity Assay

Calpain activity was performed as previously described [26] with the calpain activity kit (Abcam) according to the manufacturer's instructions.

Immunocytochemistry

Immunocytochemistry was performed as previously described [24]. Filamentous actin (F-actin) staining was performed by incubation with rhodamine phalloidin (Invitrogen). Photographs were taken with a digital camera on a Nikon Eclipse TE200, and cells with one lamellipodium or more were counted manually.

Lung Colonization Assay

Lung colonization assay was performed as we previously described [22]. Cells were harvested and injected (2×10^6 cells/0.2 ml) into the tail veins of BALB/c nude mice (Charles River, male, 8 weeks old). Three weeks after the injection, metastatic colonies on the surface of the lungs were fixed with picric acid and counted under a dissection microscope.

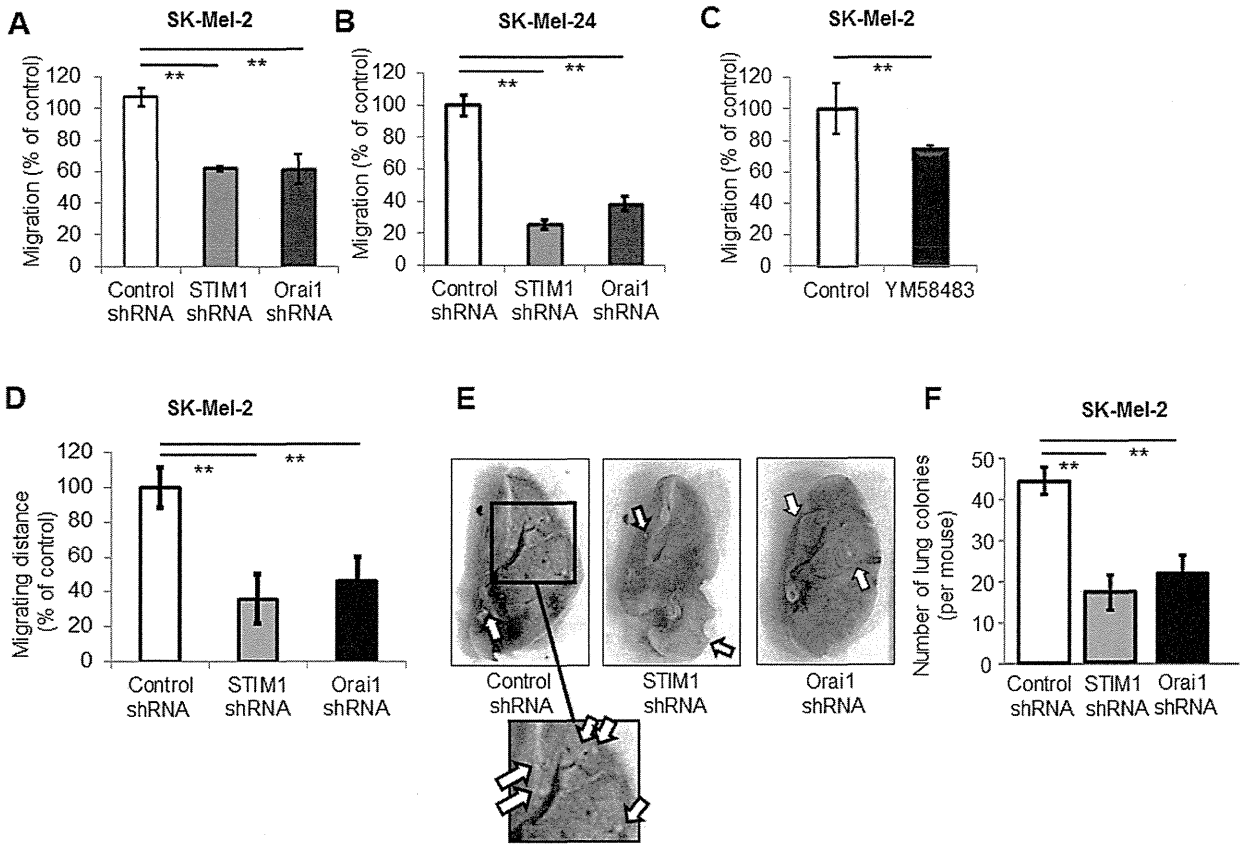

Figure 5. SOCE regulates cell migration and metastasis of melanoma. (**A and B**) Boyden chamber assay showed that either STIM1- or Orai1-knockdown inhibited cell migration. **, $p<0.01$, n = 4. (**C**) The scratch test showed that YM583483 (1 μM) inhibited cell migration. **, $p<0.01$, n = 4. (**D**) Time-lapse video recording (Videos S1, S2, and S3) showed that STIM1- or Orai1-knockdown SK-Mel-2 cells exhibited a shorter migration distance than control SK-Mel-2 cells. **, $p<0.01$, n = 10. (**E and F**) SK-Mel-2 cells with knockdown of either STIM1 or Orai1 were injected to the tail vein of Balb/c nu/nu mice. Three weeks later, the lungs were removed and fixed with picric acid. (**E**) Representative images of lung surface are shown. Arrows indicate metastatic melanoma colonies (white lesions). (**F**) The number of metastatic colonies in the lung surface was counted under a dissection microscope. **, $p<0.01$, n = 8.
doi:10.1371/journal.pone.0089292.g005

Data Analysis and Statistics

Statistical comparisons among groups were performed using Student's *t*-test or one-factor analysis of variance (ANOVA) with the Bonferroni post hoc test. The criterion of statistical significance was set at $p<0.05$. *, $p<0.05$, **, $p<0.01$, N.S., not significant.

Ethics Statement

All animal studies were approved by the Institutional Animal Care and Use Committees of New Jersey Medical School-Rutgers, The State University of New Jersey (Protocol Number: 11104D0914).

Results

STIM1 and Orai1 are Expressed in Human Melanoma

We first examined expression of STIM and Orai in human melanoma. Western blot analyses showed that STIM1 and Orai1 are expressed in metastatic human melanoma cell lines, while the melanocyte cell line, HEMA-LP, displayed only a low level of Orai1 expression (Fig. 1A and B). In contrast, STIM2, Orai2 and Orai3 expression was undetectable or barely detectable in the melanoma cell lines (data not shown). We also examined expression of STIM1 and Orai1 in human melanoma tissues, using a microarray. Both molecules were immunohistochemically detected (Fig. 1C). Interestingly, STIM1, but not Orai1, showed higher expression in metastatic melanoma than in primary melanoma (Fig. 1D). This finding was confirmed using a different set of antibodies. These data suggested that STIM1 expression, but not Orai1 expression, positively correlates with melanoma progression.

SOCE Occurs in Melanoma Cell Lines

Since STIM1 and Orai1 were detected in human melanoma tissues, we examined whether SOCE occurs in melanoma cell lines. SOCE is defined as enhanced Ca^{2+} import from extracellular space after depletion of Ca^{2+} stores in the ER. Experimentally, SOCE is induced by Ca^{2+} addition after Ca^{2+} depletion from the ER with thapsigargin (Fig. 2A), an inhibitor of sarcoplasmic reticulum Ca^{2+}-ATPase (SERCA). We observed SOCE in some melanoma and melanocyte cell lines examined (Fig. 2B). Metastatic (SK-Mel-2, C8161, SK-Mel-24 and UACC2577), but not primary (WM3248, WM115 (data not shown) and WM1552C (data not shown)), melanoma cell lines showed higher SOCE peak amplitudes than the melanocyte cell line (HEMA-LP). These data suggested that SOCE is enhanced in metastatic melanoma, in accordance with the idea that activation of SOCE is related to

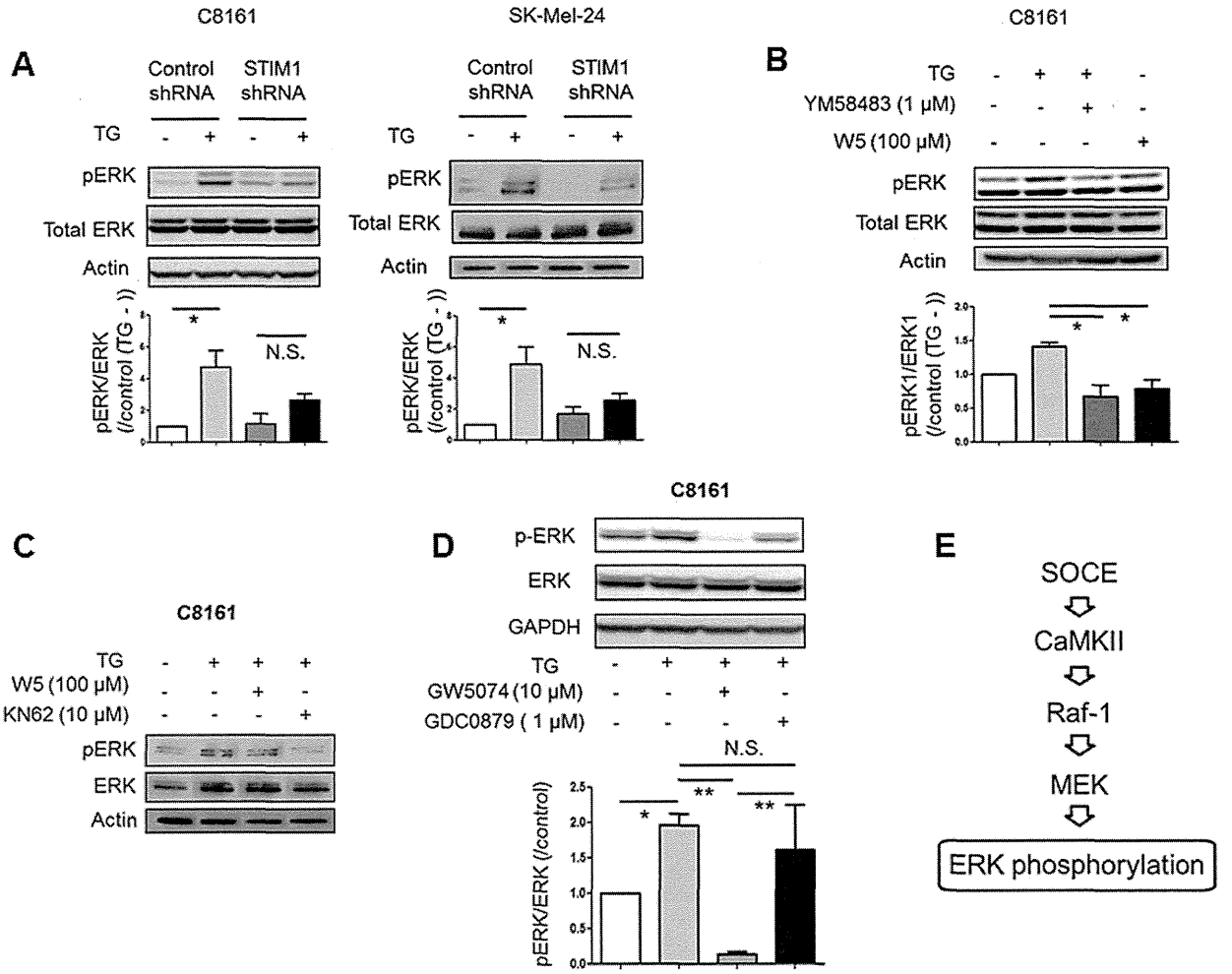

Figure 6. SOCE increases phosphorylation of ERK in melanoma. (**A**) Densitometric analyses (bar graph) of western blots show that thapsigargin increased phosphorylation of ERK1/2 in metastatic melanoma cell lines. STIM1-knockdown inhibited thapsigargin-induced phosphorylation of ERK1/2. *, $p<0.05$; N.S., not significant, n = 3. (**B**) Densitometric analyses (bar graph) of western blots show that thapsigargin-induced phosphorylation of ERK1/2 was inhibited by SOCE inhibitor YM58483 and CaM inhibitor W5 in C8161 cells. *, $p<0.05$, n = 3. (**C**) Thapsigargin-induced phosphorylation of ERK1/2 was inhibited by CaM inhibitor W5 and CaMKII inhibitor KN62 in C8161 cells. (**D**) Densitometric analyses (bar graph) of western blots show that thapsigargin-induced phosphorylation of ERK1/2 was inhibited by Raf-1 inhibitor GW5074, but not by Braf inhibitor GDC0879. *, $p<0.05$; **, $p<0.01$; N.S. not significant, n = 3. (**E**) Proposed signaling schema of SOCE-induced ERK activation.
doi:10.1371/journal.pone.0089292.g006

melanoma progression. A pyrazole compound, YM58483, which is known to inhibit SOCE in non-melanoma cells [27,28], also suppressed SOCE in metastatic melanoma cell lines (Fig. 2C and D).

STIM1- or Orai1-knockdown Inhibits SOCE in Melanoma Cell Lines

We examined whether SOCE in melanoma cell lines is regulated by STIM1 and Orai1. Ca^{2+} peak amplitude in the SOCE phase was lower in both STIM1- (Fig. 3A) and Orai1- (Fig. 3B) knockdown cells than in control metastatic melanoma cell lines (Fig. 3C). These data suggested that both STIM1 and Orai1 are involved in SOCE activation in melanoma.

Inhibition of SOCE Suppresses Melanoma Cell Proliferation

We next examined the role of SOCE in cellular functions of melanoma. We found that proliferation was reduced in STIM1-knockdown metastatic melanoma cell lines (Fig. 4A). This was not due to induction of apoptosis, because there was no significant difference of apoptosis between STIM1-knockdown and control C8161 cells after both 24 hours and 48 hours (Fig. S1). In contrast, Orai1-knockdown inhibited proliferation in C8161 cells but not in SK-Mel-2 or SK-Mel-24 cells, suggesting that STIM1, rather than Orai1, is the key determinant of melanoma proliferation. The SOCE inhibitor YM58483 (Fig. 4B) inhibited proliferation of SK-Mel-2, C8161 and SK-Mel-24 cells, further supporting the view that SOCE plays an important role in melanoma proliferation.

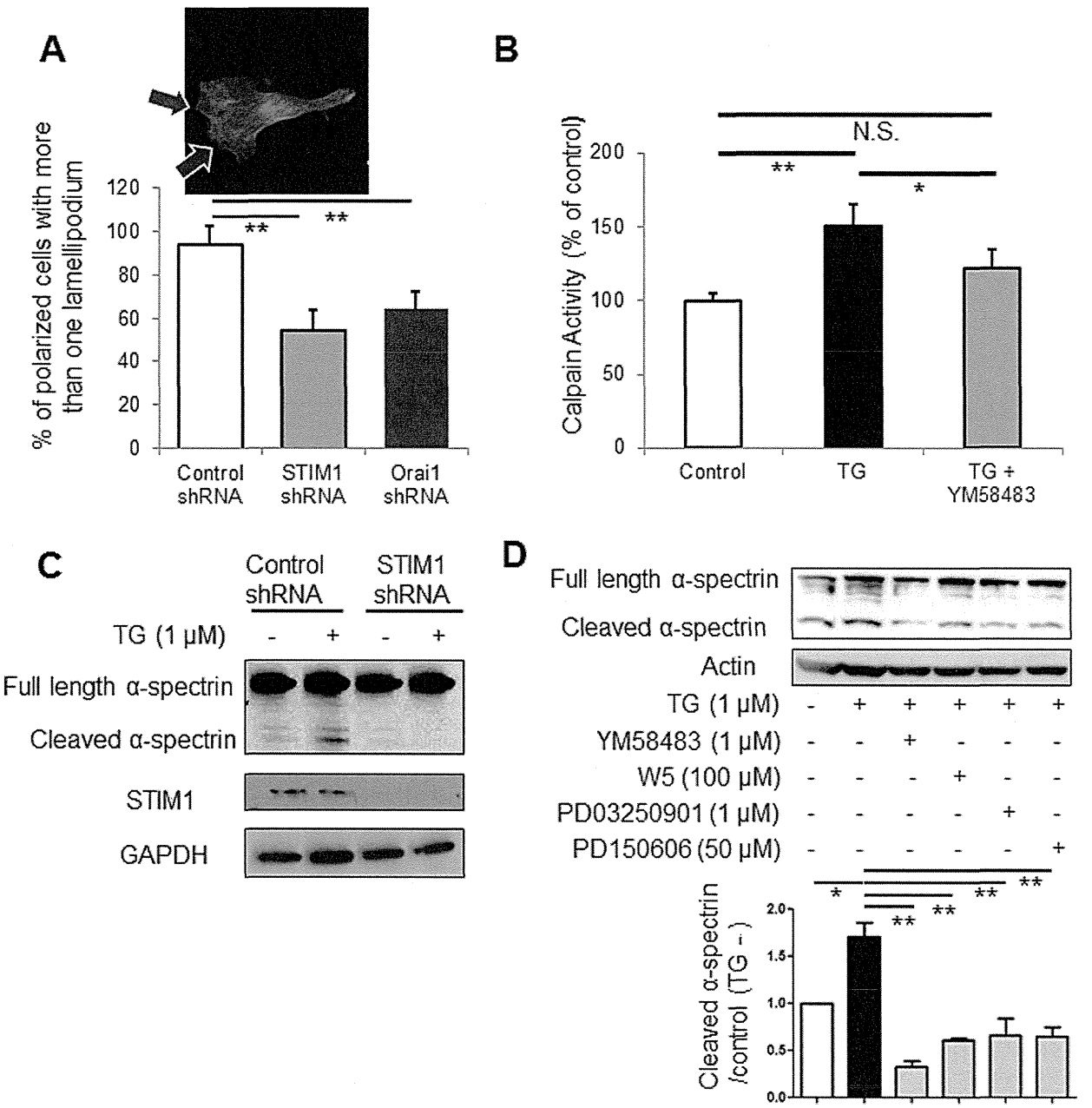

Figure 7. Proposed mechanisms of SOCE-mediated cellular functions in melanoma. (**A**) The upper panel shows actin staining of SK-Mel-2 cells. Arrows indicate lamellipodia. The lower panel shows the number of SK-Mel-2 cells with more than one lamellipodium. **, $p<0.01$, n = 331 for control shRNA, 850 for STIM1 shRNA, and 986 for Orai1 shRNA. (**B**) Calpain activity assay shows that thapsigargin increased calpain activity. Thapsigargin-induced elevation of calpain activity was inhibited by YM58483. *, $p<0.05$, **, $p<0.01$, N.S., not significant, n = 4. (**C**) Western blot analyses showed that thapsigargin (TG) increased cleavage of α-spectrin in SK-Mel-2 cells. Thapsigargin-induced cleavage of α-spectrin was inhibited by STIM1-knockdown. Representative data of 3 independent experiments are shown. (**D**) Densitometric analyses (bar graph) of western blots show that thapsigargin-induced cleavage of α-spectrin was inhibited by SOCE inhibitor YM58483, CaM inhibitor W5, MEK inhibitor PD03250901, and calpain inhibitor PD150606. *, $p<0.05$; **, $p<0.01$, n = 3.
doi:10.1371/journal.pone.0089292.g007

Inhibition of SOCE Suppresses Melanoma Cell Migration/Metastasis

Since Ca^{2+} signaling regulates migration of cancer cells [29], we also examined the role of SOCE in melanoma cell migration. We found that both STIM1- and Orai1-knockdown inhibited cell migration in metastatic melanoma cell lines (Fig. 5A and B). YM58483 also inhibited melanoma cell migration (Fig. 5C). Time-lapse video recordings showed reduced cell migration distance of both STIM1- and Orai1-knockdown cells (Fig. 5D and Videos S1, S2, and S3). We next examined whether the reduced cell migration is correlated with inhibition of metastasis. Both STIM1-

and Orai1-knockdown resulted in decreased numbers of metastatic colonies in the lungs of mice (Fig. 5E and F). These data suggested that the inhibition of SOCE suppresses melanoma cell migration and thereby reduces metastasis.

SOCE Regulates ERK Signaling in Melanoma Cell Lines

The ERK signaling pathway is known to play a major role in melanoma cells migration and proliferation [30,31]. Thus, we next examined whether SOCE affects ERK signaling. Phosphorylation of ERK1/2, which reflects activity of ERK signaling, was increased by thapsigargin in metastatic melanoma cell lines (Fig. 6A). The thapsigargin-induced ERK1/2 phosphorylation was attenuated by STIM1-knockdown (Fig. 6A) and by YM58483 (Fig. 6B), suggesting that thapsigargin-induced ERK activation occurs via a SOCE-related mechanism. Since it has been demonstrated that intracellular Ca^{2+} activates ERK signaling via calmodulin (CaM)/calmodulin-dependent protein kinase II (CaMKII) [32], we examined the involvement of these molecules in the SOCE-induced ERK activation. Thapsigargin-induced ERK1/2 phosphorylation was inhibited by W5, a CaM inhibitor (Fig. 6B and C), and by KN62, a CaMKII inhibitor (Fig. 6C), suggesting that SOCE-induced ERK activation is mediated by CaM/CaMKII. Thapsigargin-induced ERK1/2 phosphorylation was inhibited by GW5074, a specific Raf-1 inhibitor, but not by GDC0879, a specific Braf inhibitor, in C8161 cells (Fig. 6D). This is in accordance with previous findings that CaMKII can bind to and activate Raf-1 [33,34]. Similar results were also observed in SK-Mel-24 cells (data not shown), suggesting that Raf-1, rather than Braf, predominantly mediates SOCE-mediated ERK activation (Fig.6E). These data suggested that the conventional ERK signaling pathway is activated by SOCE via CaM/CaMKII.

SOCE Regulates Melanoma Cell Migration via ERK Signaling

There have been extensive studies on the mechanism of melanoma cell proliferation via ERK signaling [35,36]. However, the molecular mechanism through which ERK signaling regulates melanoma cell migration remains relatively unclear. Intracellular Ca^{2+} accelerates cell migration via calpain, a proteolytic enzyme, which promotes actin assembly/disassembly [37,38]. Therefore, it was suggested that SOCE regulates melanoma cell migration via calpain-dependent actin dynamics. This hypothesis was supported by the observation that the number of lamellipodia, which reflects the activity of actin assembly/disassembly [39,40], was decreased by STIM1- or Orai1-knockdown (Fig. 7A). In addition, we found that calpain activity was increased by thapsigargin, but was inhibited by YM58483 (Fig. 7B). Further, cleavage of α-spectrin, a target enzyme of calpain, was increased by thapsigargin, but was inhibited by STIM1-knockdown (Fig. 7C). These data suggested that SOCE regulates cell migration in a calpain-dependent manner. The question of how SOCE activates calpain then arises. Calpain was originally found as a Ca^{2+}-dependent enzyme [41], but recently it was demonstrated that ERK signaling can increase calpain activity [42–44]. We thus examined whether ERK signaling rather than intracellular Ca^{2+} itself modulates calpain activity. As shown in Fig. 7D, thapsigargin-induced α-spectrin cleavage was inhibited by YM58483, and by PD150606, a calpain inhibitor, as expected. In addition, inhibition of CaM by W5 and inhibition of MEK by PD03250901 suppressed thapsigargin-induced α-spectrin cleavage. These data suggested that calpain mediates SOCE-induced cell migration via ERK signaling, not via simple SOCE-induced elevation of intracellular Ca^{2+}.

Discussion

Our present findings show that SOCE occurs in melanoma cells and plays a pivotal role in cell proliferation and migration, most probably via ERK signaling. STIM1 and Orai1 were expressed not only in cultured melanoma cells, but also in human melanoma tissues. SOCE activity in melanoma cells was dependent on STIM1 and Orai1, and was reduced by SOCE inhibitor YM58483. Inhibition of SOCE suppressed both melanoma proliferation and cell migration. In addition, SOCE activated ERK signaling in melanoma cells, which may lead to further changes in cellular functions. Accordingly, our results suggest that melanoma progression is promoted by SOCE via ERK signaling. Recent melanoma therapies have targeted V600E-mutated Braf [1], but some patient are non-responders, and acquisition of resistance is also a problem [2]. Our data showed that SOCE occurs not only in melanoma cells bearing Braf-mutation (SK-Mel-24, UACC257, WM3248, WM115, and WM1552C), but also in non-Braf-mutation-carrying melanoma cells lines (SK-Mel-2 and C8161). In addition, we found that STIM1-knockdown inhibited ERK phosphorylation in both Braf-mutated (SK-Mel-24) and non-Braf-mutated (SK-Mel-2 and C8161) cells. These data suggested that inhibition of SOCE suppresses ERK signaling activity irrespective of the existence of Braf mutation. Therefore, targeting SOCE could potentially benefit a greater number of melanoma patients, compared to currently used Braf inhibitors.

The role of SOCE in proliferation and cell migration is well established. Abdullaev *et al.* showed that STIM1 and Orai1 regulate CRAC currents and SOCE, leading to changes in proliferation of endothelial cells [11]. In vascular smooth muscle cells, knockdown of either STIM1 or Orai1, but not of STIM2, Orai2, and Orai3, inhibited proliferation and cell migration [13]. In cancer cells, Yang *et al.* reported that STIM1-knockdown inhibited serum-induced breast tumor cell migration [16]. The same group also showed that STIM1-knockdown in hepatocarcinoma cells affects disassembly and turnover of focal adhesion [45]. Our data demonstrate that STIM1 and Orai1 have roles in proliferation and migration of various melanoma cell lines, indicating that SOCE contributes to melanoma progression. Orai1 knockdown had only a minor effect on proliferation compared to STIM1 knockdown, suggesting that TRPC channels rather than Orai1 potentially interact with STIM [46] in the regulation of proliferation. There was a discrepancy between the effective concentrations of YM58483 for inhibition of proliferation and inhibition of SOCE. This can be attributed, at least in part, to compensatory upregulation of SOCE [47], which would occur during the relatively prolonged exposure to the SOCE-inhibitory drug in MTT assay compared to the short exposure during SOCE measurement. Another concern is the fact that Orai1 deletion did not inhibit proliferation of SK-Mel-2 and SK-Mel-24 cells, whereas YM58483 treatment did. This might be explained by incomplete knockdown of Orai1.

It was recently demonstrated that, in mouse melanoma cells, SOCE occurs in lipid rafts, and ablation of the rafts suppressed tumor growth, most probably via the Akt pathway [48]. These data, taken together with ours, indicate that SOCE regulates multiple pathways in melanoma, supporting our proposal that SOCE plays a pivotal role in melanoma progression.

The upstream pathway leading to SOCE in melanoma cells remains unknown. Ca^{2+} depletion in the ER is mainly controlled by the phospholipase C (PLC)/IP_3/IP_3 receptor pathway, which is generally activated by either tyrosine kinase-type receptors or Gq-related G protein coupled receptors. Previous reports indicated that SOCE is controlled by tyrosine kinase-type receptors rather

than Gq-coupled receptors. For example, in colorectal cancer cells, epidermal growth factor (EGF) increased expression of cyclooxygenase-2 via STIM1 and Orai1 [49]. In pulmonary arterial smooth muscle cells, platelet-derived growth factor (PDGF) activated SOCE via Akt signaling [50]. In addition, both EGF [51] and PDGF [52] can increase the activity of ERK signaling in melanoma. It will be interesting to investigate the functional relationship among tyrosine kinase-type receptors, SOCE and the ERK signaling in melanoma cells.

In conclusion, our results indicate that inhibition of SOCE suppressed proliferation and cell migration/metastasis of melanoma cells, most probably via ERK signaling. We propose that SOCE is a potential target for treatment of melanoma, irrespective of whether or not Braf mutation is present.

Supporting Information

Figure S1 STIM1-knockdown did not promote apoptosis. APC Annexin V and 7-AAD staining assays demonstrated that apoptosis of STIM1-knockdown and control shRNA-transduced C8161 cells was not different. These data demonstrate that apoptosis did not contribute to the STIM1-knockdown-induced inhibition of cell proliferation. N.S. not significant, n = 4.
(TIF)

Video S1 Melanoma cell migration was inhibited by STIM1- or by Orai1-knockdown. Cellular movement was recorded by time-lapse video microscopy recording. Video S1, control shRNA, video S2, STIM1 shRNA, video S3, Orai1 shRNA.
(WMV)

Video S2 Melanoma cell migration was inhibited by STIM1- or by Orai1-knockdown. Cellular movement was recorded by time-lapse video microscopy recording. Video S1, control shRNA, video S2, STIM1 shRNA, video S3, Orai1 shRNA.
(WMV)

Video S3 Melanoma cell migration was inhibited by STIM1- or by Orai1-knockdown. Cellular movement was recorded by time-lapse video microscopy recording. Video S1, control shRNA, video S2, STIM1 shRNA, video S3, Orai1 shRNA.
(WMV)

Acknowledgments

The authors are grateful to Akane Nagasako for technical assistance in this study.

Author Contributions

Conceived and designed the experiments: MU YI KI. Performed the experiments: MU EB LX XF KO AM. Analyzed the data: MU EB SF MSD XF MI. Contributed reagents/materials/analysis tools: SF MD LX UY TF SC JG. Wrote the paper: MU EB SFD LX MI YI KI.

References

1. Chapman PB, Hauschild A, Robert C, Haanen JB, Ascierto P, et al. (2011) Improved Survival with Vemurafenib in Melanoma with BRAF V600E Mutation. New England Journal of Medicine 364: 2507–2516.
2. Nazarian R, Shi H, Wang Q, Kong X, Koya RC, et al. (2010) Melanomas acquire resistance to B-RAF(V600E) inhibition by RTK or N-RAS upregulation. Nature 468: 973–977.
3. Berridge MJ, Bootman MD, Roderick HL (2003) Calcium signalling: dynamics, homeostasis and remodelling. Nat Rev Mol Cell Biol 4: 517–529.
4. Putney JW (2005) Capacitative calcium entry: sensing the calcium stores. The Journal of Cell Biology 169: 381–382.
5. Feske S, Gwack Y, Prakriya M, Srikanth S, Puppel S-H, et al. (2006) A mutation in Orai1 causes immune deficiency by abrogating CRAC channel function. Nature 441: 179–185.
6. Prakriya M, Feske S, Gwack Y, Srikanth S, Rao A, et al. (2006) Orai1 is an essential pore subunit of the CRAC channel. Nature 443: 230–233.
7. Oh-hora M, Yamashita M, Hogan PG, Sharma S, Lamperti E, et al. (2008) Dual functions for the endoplasmic reticulum calcium sensors STIM1 and STIM2 in T cell activation and tolerance. Nat Immunol 9: 432–443.
8. Baba Y, Kurosaki T (2009) Physiological function and molecular basis of STIM1-mediated calcium entry in immune cells. Immunological Reviews 231: 174–188.
9. Di Capite J, Parekh AB (2009) CRAC channels and Ca2+ signaling in mast cells. Immunological Reviews 231: 45–58.
10. Baba Y, Hayashi K, Fujii Y, Mizushima A, Watarai H, et al. (2006) Coupling of STIM1 to store-operated Ca2+ entry through its constitutive and inducible movement in the endoplasmic reticulum. Proceedings of the National Academy of Sciences 103: 16704–16709.
11. Abdullaev IF, Bisaillon JM, Potier M, Gonzalez JC, Motiani RK, et al. (2008) Stim1 and Orai1 Mediate CRAC Currents and Store-Operated Calcium Entry Important for Endothelial Cell Proliferation. Circulation Research 103: 1289–1299.
12. Bisaillon JM, Motiani RK, Gonzalez-Cobos JC, Potier M, Halligan KE, et al. (2010) Essential role for STIM1/Orai1-mediated calcium influx in PDGF-induced smooth muscle migration. American Journal of Physiology - Cell Physiology 298: C993–C1005.
13. Potier M, Gonzalez JC, Motiani RK, Abdullaev IF, Bisaillon JM, et al. (2009) Evidence for STIM1- and Orai1-dependent store-operated calcium influx through ICRAC in vascular smooth muscle cells: role in proliferation and migration. The FASEB Journal 23: 2425–2437.
14. Suyama E, Wadhwa R, Kaur K, Miyagishi M, Kaul SC, et al. (2004) Identification of Metastasis-related Genes in a Mouse Model Using a Library of Randomized Ribozymes. Journal of Biological Chemistry 279: 38083–38086.
15. Chen Y-F, Chiu W-T, Chen Y-T, Lin P-Y, Huang H-J, et al. (2011) Calcium store sensor stromal-interaction molecule 1-dependent signaling plays an important role in cervical cancer growth, migration, and angiogenesis. Proceedings of the National Academy of Sciences 108: 15225–15230.
16. Yang S, Zhang JJ, Huang X-Y (2009) Orai1 and STIM1 Are Critical for Breast Tumor Cell Migration and Metastasis. Cancer cell 15: 124–134.
17. Fedida-Metula S, Feldman B, Koshelev V, Levin-Gromiko U, Voronov E, et al. (2012) Lipid rafts couple store-operated Ca2+ entry to constitutive activation of PKB/Akt in a Ca2+/calmodulin-, Src- and PP2A-mediated pathway and promote melanoma tumor growth. Carcinogenesis 33: 740–750.
18. Varga-Szabo D, Braun A, Kleinschnitz C, Bender M, Pleines I, et al. (2008) The calcium sensor STIM1 is an essential mediator of arterial thrombosis and ischemic brain infarction. The Journal of Experimental Medicine 205: 1583–1591.
19. McCarl C-A, Picard C, Khalil S, Kawasaki T, Röther J, et al. (2009) ORAI1 deficiency and lack of store-operated Ca2+ entry cause immunodeficiency, myopathy, and ectodermal dysplasia. Journal of Allergy and Clinical Immunology 124: 1311–1318.e1317.
20. Hoeflich KP, Herter S, Tien J, Wong L, Berry L, et al. (2009) Antitumor Efficacy of the Novel RAF Inhibitor GDC-0879 Is Predicted by BRAFV600E Mutational Status and Sustained Extracellular Signal-Regulated Kinase/Mitogen-Activated Protein Kinase Pathway Suppression. Cancer Research 69: 3042–3051.
21. Iwatsubo K, Minamisawa S, Tsunematsu T, Nakagome M, Toya Y, et al. (2004) Direct Inhibition of Type 5 Adenylyl Cyclase Prevents Myocardial Apoptosis without Functional Deterioration. Journal of Biological Chemistry 279: 40938–40945.
22. Baljinnyam E, Umemura M, De Lorenzo MS, Iwatsubo M, Chen S, et al. (2011) Epac1 promotes melanoma metastasis via modification of heparan sulfate. Pigment Cell & Melanoma Research 24: 680–687.
23. Yokoyama U, Ishiwata R, Jin M-H, Kato Y, Suzuki O, et al. (2012) Inhibition of EP4 Signaling Attenuates Aortic Aneurysm Formation. PLoS ONE 7: e36724.
24. Baljinnyam E, De Lorenzo MS, Xie L-H, Iwatsubo M, Chen S, et al. (2010) Exchange Protein Directly Activated by Cyclic AMP Increases Melanoma Cell Migration by a Ca2+-Dependent Mechanism. Cancer Research 70: 5607–5617.
25. Baljinnyam E, Iwatsubo K, Kurotani R, Wang X, Ulucan C, et al. (2009) Epac increases melanoma cell migration by a heparan sulfate-related mechanism. American journal of physiology Cell physiology 297: C802–813.
26. Mattheij NJA, Gilio K, van Kruchten R, Jobe SM, Wieschhaus AJ, et al. (2013) Dual Mechanism of Integrin αIIbβ3 Closure in Procoagulant Platelets. Journal of Biological Chemistry 288: 13325–13336.
27. Ishikawa J, Ohga K, Yoshino T, Takezawa R, Ichikawa A, et al. (2003) A Pyrazole Derivative, YM-58483, Potently Inhibits Store-Operated Sustained Ca2+ Influx and IL-2 Production in T Lymphocytes. The Journal of Immunology 170: 4441–4449.
28. He L-P, Hewavitharana T, Soboloff J, Spassova MA, Gill DL (2005) A Functional Link between Store-operated and TRPC Channels Revealed by the

3,5-Bis(trifluoromethyl)pyrazole Derivative, BTP2. Journal of Biological Chemistry 280: 10997–11006.
29. Hordijk PL (2006) Endothelial signalling events during leukocyte transmigration. FEBS Journal 273: 4408–4415.
30. Zhang W, Liu HT (2002) MAPK signal pathways in the regulation of cell proliferation in mammalian cells. Cell Res 12: 9–18.
31. McCubrey JA, Steelman LS, Chappell WH, Abrams SL, Wong EWT, et al. (2007) Roles of the Raf/MEK/ERK pathway in cell growth, malignant transformation and drug resistance. Biochimica et Biophysica Acta (BBA) - Molecular Cell Research 1773: 1263–1284.
32. Agell N, Bachs O, Rocamora N, Villalonga P (2002) Modulation of the Ras/Raf/MEK/ERK pathway by Ca2+, and Calmodulin. Cellular Signalling 14: 649–654.
33. Illario M, Cavallo AL, Bayer KU, Di Matola T, Fenzi G, et al. (2003) Calcium/Calmodulin-dependent Protein Kinase II Binds to Raf-1 and Modulates Integrin-stimulated ERK Activation. Journal of Biological Chemistry 278: 45101–45108.
34. Salzano M, Rusciano MR, Russo E, Bifulco M, Postiglione L, et al. (2012) Calcium/calmodulin-dependent protein kinase II (CaMKII) phosphorylates Raf-1 at serine 338 and mediates Ras-stimulated Raf-1 activation. Cell Cycle 11: 2100–2106.
35. Sullivan RJ, Atkins MB (2010) Molecular targeted therapy for patients with melanoma: the promise of MAPK pathway inhibition and beyond. Expert Opinion on Investigational Drugs 19: 1205–1216.
36. Meier F, Schittek B, Busch S, Garbe C, Smalley K, et al. (2005) The RAS/RAF/MEK/ERK and PI3K/AKT signaling pathways present molecular targets for the effective treatment of advanced melanoma. Frontiers in bioscience : a journal and virtual library 10: 2986–3001.
37. Potter DA, Srirangam A, Fiacco KA, Brocks D, Hawes J, et al. (2003) Calpain regulates enterocyte brush border actin assembly and pathogenic Escherichia coli-mediated effacement. J Biol Chem 278: 30403–30412.
38. Huang C, Rajfur Z, Yousefi N, Chen Z, Jacobson K, et al. (2009) Talin phosphorylation by Cdk5 regulates Smurf1-mediated talin head ubiquitylation and cell migration. Nat Cell Biol 11: 624–630.
39. Ohashi K, Fujiwara S, Watanabe T, Kondo H, Kiuchi T, et al. (2011) LIM kinase has a dual role in regulating lamellipodium extension by decelerating the rate of actin retrograde flow and the rate of actin polymerization. J Biol Chem 286: 36340–36351.
40. Batchelder EL, Hollopeter G, Campillo C, Mezanges X, Jorgensen EM, et al. (2011) Membrane tension regulates motility by controlling lamellipodium organization. Proc Natl Acad Sci U S A 108: 11429–11434.
41. Dayton WR, Goll DE, Zeece MG, Robson RM, Reville WJ (1976) A Ca2+-activated protease possibly involved in myofibrillar protein turnover. Purification from porcine muscle. Biochemistry 15: 2150–2158.
42. Chen H, Libertini SJ, Wang Y, Kung HJ, Ghosh P, et al. (2010) ERK regulates calpain 2-induced androgen receptor proteolysis in CWR22 relapsed prostate tumor cell lines. J Biol Chem 285: 2368–2374.
43. Glading A, Uberall F, Keyse SM, Lauffenburger DA, Wells A (2001) Membrane proximal ERK signaling is required for M-calpain activation downstream of epidermal growth factor receptor signaling. J Biol Chem 276: 23341–23348.
44. Glading A, Chang P, Lauffenburger DA, Wells A (2000) Epidermal growth factor receptor activation of calpain is required for fibroblast motility and occurs via an ERK/MAP kinase signaling pathway. J Biol Chem 275: 2390–2398.
45. Yang N, Tang Y, Wang F, Zhang H, Xu D, et al. (2013) Blockade of store-operated Ca2+ entry inhibits hepatocarcinoma cell migration and invasion by regulating focal adhesion turnover. Cancer Letters.
46. Yuan JP, Kim MS, Zeng W, Shin DM, Huang G, et al. (2009) TRPC channels as STIM1-regulated SOCs. Channels 3: 221–225.
47. Darbellay B, Arnaudeau S, König S, Jousset H, Bader C, et al. (2009) STIM1- and Orai1-dependent Store-operated Calcium Entry Regulates Human Myoblast Differentiation. Journal of Biological Chemistry 284: 5370–5380.
48. Fedida-Metula S, Feldman B, Koshelev V, Levin-Gromiko U, Voronov E, et al. (2012) Lipid rafts couple store-operated Ca2+ entry to constitutive activation of PKB/Akt in a Ca2+/calmodulin-, Src- and PP2A-mediated pathway and promote melanoma tumor growth. Carcinogenesis 33: 740–750.
49. Wang J-Y, Chen B-K, Wang Y-S, Tsai Y-T, Chen W-C, et al. (2012) Involvement of store-operated calcium signaling in EGF-mediated COX-2 gene activation in cancer cells. Cellular Signalling 24: 162–169.
50. Ogawa A, Firth AL, Smith KA, Maliakal MV, Yuan JX-J (2012) PDGF enhances store-operated Ca2+ entry by upregulating STIM1/Orai1 via activation of Akt/mTOR in human pulmonary arterial smooth muscle cells. American Journal of Physiology - Cell Physiology 302: C405–C411.
51. Ivanov VN, Hei TK (2004) Combined treatment with EGFR inhibitors and arsenite upregulated apoptosis in human EGFR-positive melanomas: a role of suppression of the PI3K-AKT pathway. Oncogene 24: 616–626.
52. Pirraco A, Coelho P, Rocha A, Costa R, Vasques L, et al. (2010) Imatinib targets PDGF signaling in melanoma and host smooth muscle neighboring cells. Journal of Cellular Biochemistry 111: 433–441.

Protection of Cardiomyocytes from the Hypoxia-Mediated Injury by a Peptide Targeting the Activator of G-Protein Signaling 8

Motohiko Sato[1]*, Masahiro Hiraoka[2], Hiroko Suzuki[1], Miho Sakima[1], Abdullah Al Mamun[1], Yukiko Yamane[2], Takayuki Fujita[2], Utako Yokoyama[2], Satoshi Okumura[3], Yoshihiro Ishikawa[2]

1 Department of Physiology, Aichi Medical University, Nagakute, Aichi, Japan, **2** Cardiovascular Research Institute, Yokohama City University School of Medicine, Fukuura, Yokohama, Japan, **3** Department of Physiology, Tsurumi University School of Dental Medicine, Yokohama, Japan

Abstract

Signaling via heterotrimeric G-protein is involved in the development of human diseases including ischemia-reperfusion injury of the heart. We previously identified an ischemia-inducible G-protein activator, activator of G-protein signaling 8 (AGS8), which regulates Gβγ signaling and plays a key role in the hypoxia-induced apoptosis of cardiomyocytes. Here, we attempted to intervene in the AGS8-Gβγ signaling process and protect cardiomyocytes from hypoxia-induced apoptosis with a peptide that disrupted the AGS8-Gβγ interaction. Synthesized AGS8-peptides, with amino acid sequences based on those of the Gβγ-binding domain of AGS8, successfully inhibited the association of AGS8 with Gβγ. The AGS8-peptide effectively blocked hypoxia-induced apoptosis of cardiomyocytes, as determined by DNA end-labeling and an increase in cleaved caspase-3. AGS8-peptide also inhibited the change in localization/permeability of channel protein connexin 43, which was mediated by AGS8-Gβγ under hypoxia. Small compounds that inhibit a wide range of Gβγ signals caused deleterious effects in cardiomyocytes. In contrast, AGS8-peptide did not cause cell damage under normoxia, suggesting an advantage inherent in targeted disruption of the AGS8-Gβγ signaling pathway. These data indicate a pivotal role for the interaction of AGS8 with Gβγ in hypoxia-induced apoptosis of cardiomyocytes, and suggest that targeted disruption of the AGS8-Gβγ signal provides a novel approach for protecting the myocardium against ischemic injury.

Citation: Sato M, Hiraoka M, Suzuki H, Sakima M, Mamun AA, et al. (2014) Protection of Cardiomyocytes from the Hypoxia-Mediated Injury by a Peptide Targeting the Activator of G-Protein Signaling 8. PLoS ONE 9(3): e91980. doi:10.1371/journal.pone.0091980

Editor: Xin-Liang Ma, Thomas Jefferson University, United States of America

Received December 10, 2013; **Accepted** February 16, 2014; **Published** March 14, 2014

Funding: This work is supported by Grant-in-Aid for Scientific Research on Innovative Areas of Japan (MS), Grant-in-Aid for Scientific Research of Japan (MS), the Toyoaki Scholarship Foundation (MS), The Naito Foundation (MS) and Strategic Research Foundation Grant-aided Project for Private Universities from the Ministry of Education, Culture, Sports, Science, and Technology, Japan (MEXT), 2011–2015 (S1101027). The funders had no role in study design, data collection and analysis, decision to publish, or preparation of the manuscript.

Competing Interests: The authors have declared that no competing interests exist.

* E-mail: motosato@aichi-med-u.ac.jp

Introduction

Signaling mediated by heterotrimeric G-protein plays important roles in signal integration in cells. Heterotrimeric G-proteins are activated by G-protein–coupled receptors (GPCRs) at the cell surface in response to extra stimuli. The activation of G-protein signaling is associated with nucleotide exchange on the Gα subunits leading to a conformational change in Gαβγ and subsequent transduction of signals to various effector molecules [1]. However, a novel class of regulatory proteins that directly activate heterotrimeric G protein without receptor activation has been identified [2–4]. Such molecules are expected to provide alternative signaling via heterotrimeric G-protein and regulate signal adaptation during pathophysiologic stress [5].

The importance of accessory proteins for heterotrimeric G-protein has been reported in human diseases and animal models [5]. For example, activator of G-protein signaling 1 (AGS1) is a direct activator of the Gα subunit and involved in the secretion of atrial natriuretic factor in heart failure [6,7]. Further, regulators of G-protein signaling (RGSs), the group of proteins that inhibit G-protein signaling by accelerating the GTPase activity of the Gα subunit, are involved in various cardiovascular diseases, such as hypertension, cardiac hypertrophy, and hypoxia-mediated injury [8–10].

We have been focusing on identification of accessory proteins of heterotrimeric G-proteins induced in cardiovascular diseases and have found novel activators of G-protein signaling from the hypertrophied heart and during repetitive transient ischemia [11,12]. Thus, we identified TFE3 (AGS11), an AGS protein that selectively forms a complex with the Gα16 subunit and is upregulated in the hypertrophied hearts of mice [11]. TFE3 translocates Gα16 to the nucleus, which leads to the induction of claudin-14, a component of the membrane in cardiomyocytes. This suggests that the novel form of transcriptional regulation counteracts pressure overload.

Activator of G-protein signaling 8 (AGS8) is a Gβγ signal regulator isolated from a cDNA library of rat hearts subjected to repetitive transient ischemia [12]. In response to hypoxia, AGS8 is up-regulated in the myocardium and cultured adult cardiomyocytes. AGS8 interacts directly with Gβγ and promotes Gβγ signaling in cells [12]. Suppression of AGS8 inhibits hypoxia-induced apoptosis of cardiomyocytes, suggesting AGS8 is required for hypoxia-mediated cell death [13]. AGS8 complexes with

connexin 43 (CX43) to form a transmembrane channel for multiple small molecules, including calcium, adenosine, ATP, and reactive oxygen species [14–16]. AGS8 regulates phosphorylation of CX43 in a Gβγ-dependent manner and influences hypoxia-mediated internalization of cell-surface CX43 [13]. Therefore, the AGS8-Gβγ complex plays a critical role under hypoxic conditions, making the cellular environment more sensitive to hypoxic stress by influencing the permeability of molecules passing through CX43.

Ischemic injury of the heart is associated with activation of multiple signal cascades initiating intracellular ionic and chemical changes that lead to the death of cardiomyocytes [17,18]. A previous study indicated that AGS8-Gβγ is involved in the programs leading to cell death, and the formation of the AGS8-Gβγ complex appears to be a critical step triggering the apoptotic process [13]. If a tool to manipulate the AGS8-Gβγ interaction in cells were available, it might be a promising approach for protection of cardiomyocytes against hypoxia-mediated injury.

Here, we report the identification of the Gβγ-interface of AGS8 and a peptide (AGS8-peptide) designed to correspond to the domain of interaction between Gβγ and AGS8 that protects cardiomyocytes against hypoxia-induced apoptosis. The observations indicate the importance of the AGS8-Gβγ complex in hypoxia-mediated apoptosis of cardiomyocytes as well as the potential value of targeted disruption of the AGS8-Gβγ signal for protecting the myocardium against ischemic injury.

Experimental Procedures

Materials

Anti Gβ antibody was obtained from Santa Cruz Biotechnology. Anti CX43 antibody and IGEPAL CA-630 was obtained from Sigma. Gallein was purchased from Calbiochem. Cleaved caspase-3 andtibody was obtained from Cell Signaling Technology. Recombinant $G\beta_1\gamma_2$ was obtained from Calbiochem-Merck Millipore. MTT (3-(4,5-methylthiazol-2-yl)-2,5-diphenyltetrazolium bromide) was purchased from Dojindo Molecular Laboratories (Kumamoto, Japan).

Synthesis of Peptide

The peptides were synthesized and purified by Invitrogen and peptide identity was verified by matrix-assisted laser desorption ionization mass spectrometry. The peptides were dissolved in aliquots (10 mM) and immediately frozen at −70°C.

Generation of GST-fusion Protein, Protein Interaction Assays, and Immunoblotting

The segments of AGS8 (DQ256268) were amplified by PCR and fused in frame to GST in the pGEX-6T vector (Amersham Biotech). Each GST-partial-AGS8 fusion proteins were expressed in bacteria (*Escherichia coli* BL21, Amersham Biotech) and purified on a glutathione affinity matrix. The GST fusion protein was eluted from the resin, and glutathione was removed by desalting to allow a solution-phase interaction assay [19]. Protein interaction assays and immunoblotting were performed as described previously [19,20].

Preparation of Cardiomyocytes and Delivery of Peptide to Cells

Cardiomyocytes were prepared from the hearts of 1-3-day-old Wistar rats as described previously [13]. The neonates were deeply anesthetized with pentobarbital sodium (100 mg/kg) and decapitated for cardiac tissue harvesting. The ventricular cardiomyocytes were then enzymentically dissociated and seeded at 1.0×10^5 cell in 24 mm or 4.0×10^5 cell in 35 mm plates. Prepared cardiomyocytes were cultured in DMEM/F12 including Insulin–Transferrin–Selenite (ITS), 100 units/ml penicillin, 100 mg/ml streptomycin, and 10 mM glutamine, in 5% CO_2 at 37°C. In some experiments, cardiomyocytes were incubated in a hypoxic incubator (MODEL9200, Wakenyaku, Kyoto, Japan) equilibrated to 1% O_2, 5% CO_2, and 94% N_2 at 37°C. The cells were subjected to two different hypoxic challenges. In the first protocol, cardiomyocytes were exposed 3 times to 30 min of hypoxia with intermittent 30-min periods of normoxia to capture the early events caused by hypoxia in the living cells before they died. Particularly, internalization of cell-surface connexin 43 and changes in the permeability of connexin were analyzed. In the second protocol, cardiomyocytes were exposed to 1% O_2 for 6 h followed by 12 h of normoxia to induce hypoxia-mediated apoptosis. At the end of the second protocol, apoptotic cell death was analyzed. In some experiments, approximately 24 h after preparation, peptides were delivered to cardiomyocytes by using PLUSin (Polyplus, NY, USA) according to the manufacturer's instructions. Briefly, ~1.0 μg peptide was incubated with 2.0 μl of PLUSin in 100 μl supplied buffer for 15 min and then added the mixture to each dishes. This preparation typically provided 0.5 to 1 μM of peptide in the culture medium. The amount of peptide and the incubation time for peptide-delivery were optimized by analyzing incorporation of fluorescein isothiocyanate (FITC)-conjugated peptide into cardiomyocytes. In the condition used in this study, the chemical reagent for peptide delivery did not influence the number of living cells analyzed by trypan blue stain within 4 h treatment (0.75 μM peptide; 102.0±6.7%, 1.5 μM peptide; 90.5±5.0% versus no treatment control, not statistically significant, n = 4) [21].

Immunocytochemistry

Immunostaing of cultured cardiomyocytes was performed as described previously [13]. Briefly, cells were seeded on 24×24 mm polylysine-coated coverslips. Cells were fixed with 4% paraformaldehyde for 15 min and then incubated with 0.2% Triton X-100 for 5 min. After 1 h incubation of 5% normal donkey serum, cells were incubated with primary antibodies for 18 h at 4°C. Following 1 h incubation of secondary antibody (goat anti-mouse AlexaFluor 488 or goat anti-rabbit AlexaFluor 594, highly cross-absorbed, Molecular Probes), cells were incubated with 1 μg/ml 4′,6′-diamidino-2-phenylindole, dihydrochloride (DAPI) (Molecular Probes) in PBS for 5 min. Slides were then mounted with glass coverslips with ProLong Gold antifade reagent (Invitrogen). Images were analyzed by deconvolution microscopy (TE2000-E, Nikon, Tokyo, Japan). Obtained images were deconvoluted using NIS-Elements 3.0 software (Nikon) with a "no neighbors" deconvolution algorithm. All images were obtained from approximately the middle plane of the cells.

Dye Uptake Study

Up take of CX43 permeable fluorescence dye Lucifer Yellow (LY) (Molecular Probes) was performed as described previously [13]. Briefly, cardiomyocytes were incubated with 1 mM Lucifer Yellow (LY) (Molecular Probes) for 30 min. The fluorescence of LY was determined by fluorescence microscopy (B-3A filter, TE2000-E, NIKON, Tokyo, Japan) following removal of incorporated LY and rinse with PBS. The signal intensity was quantified in 10 randomly selected fields (10×20) using NIS-Elements 3.0 software (NIKON, Tokyo, Japan). The non-specific binding of LY was determined in the presence of a connexin hemichannel blocker, 50 mM of Lanthanum (Sigma-Aldrich).

In situ Assay for Apoptosis Detection

In situ labeling of fragmented DNA in cardiac myocytes was detected by TACS2 TdT-Blue Label In Situ Apoptosis Detection Kit (Travigen, Inc., Gaitherburg, MD), that detects DNA breaks in genomic DNA by enzymatic incorporation of biotinylated nucleotides followed by the binding of streptavidin-peroxidase conjugates, according to the manufacture's instructions. Briefly, myocytes were fixed with 3.7% formaldehyde in phosphate buffered saline (PBS) for 10 min and with 70% ethanol for 5 min and then incubated in proteinase K (0.02 mg/ml) at room temperature for 5 min. The cells were incubated with 2% hydrogen peroxide for 5 min and washed with labeling buffer consisting of 50 mM Tris (pH 7.5), 5 mM $MgCl_2$, 60 mM 2-mercaptoethanesulfonic acid, and 0.05% BSA, followed by 60 min of incubation at 37°C in labeling buffer containing 150 mM dATP, 150 mM dGTP, 150 mM dTTP, 5 mM biotinylated dCTP, and 40 U/ml of the Klenow fragment of DNA polymerase I. Untreated myocytes incubated with or without 2 mg/ml DNAse in the labeling buffer were used as positive or negative controls, respectively. The incorporated biotinylated dCTP was then detected with strepavidin-peroxidase conjugate and revealed in 0.5 mg/ml diaminobenzidine for 10 min. Nuclear brown staining was viewed under a light microscope.

MTT Assay

Cardiomyocytes in 24-well culture plates were incubated in PBS (pH 7.4) containing 0.5 mg/ml MTT at 37°C. After for 2 h incubation, the PBS was removed and 100 µl of dimethyl sulfoxide (DMSO) was added to each well to solubilize dark blue formazan products. Absorbance of the colored solution was determined at 595 nm [22].

Miscellaneous Procedures and Statistical Analysis

Immunoblotting and data analysis were performed as described previously [12,13]. The luminescence images captured with an image analyzer (LAS-3000, Fujifilm, Tokyo, Japan) were quantified using Image Gauge 3.4 (Fujifilm). Data are expressed as mean ± S.E.M. from independent experiments as described in the figure legends. Statistical analyses were performed using the unpaired *t* test, F-test, one-way ANOVA followed by Tukey's multiple comparison post-hoc test. All statistical analyses were performed with Prism 4 (GraphPad Software, USA).

Ethics Statement

Animal study was approved by the Institutional Animal Care and Use Committees of Yokohama City University.

Results

The C-terminal Region of AGS8 was Required to Activate Gβγ Signaling in Cells

To determine the region of interaction between Gβγ and AGS8, we divided the rat AGS8 (DQ256268) sequence into 6 segments and synthesized the segments as glutathione *S*-transferase (GST)-fusion proteins (Fig. 1*A*). Each of GST-AGS8 peptides was subjected to a pull-down assay to examine its interaction with purified Gβγ (Fig. 1*B*). The C-terminus of AGS8 (AGS8-C) successfully pulled down Gβγ, as documented in the previous manuscript [12]. Another segment, AGS8-254, also pulled down Gβγ to a lesser extent than AGS8-C, suggesting that a potential second Gβγ-interacting domain existed in this region. However, the remaining segments failed to pull down Gβγ.

Next, the bioactivity of each of the AGS8 regions was investigated by evaluating the activation the G-protein signaling pathway in Saccharomyces *cerevisiae* [12,23]. This yeast strain lacked the pheromone receptor, but expressed mammalian Gαs in place of the yeast Gα subunit and provided a read-out of growth upon activation of the G-protein–regulated pheromone signaling pathway [23]. The peptide corresponding to each AGS8 domain was subcloned in a galactose-inducible vector and introduced into the yeast strain [24]. The bioactivity in the G-protein pathway was examined be evaluating the galactose-dependent growth of the transformed yeast. Although each segment of AGS8 was expressed in the yeast cells, AGS8-C was the only segment able to activate G-protein signaling (Fig. 1*C*). Thus, we focused on AGS-C and explored the Gβγ-interaction site in this domain.

The FN3 Domain was Important for the Interaction of AGS8 with Gβγ

The sequence of AGS8-C (A^{1359} to W^{1730} of rat ABB82299) was further divided into smaller fragments that were synthesized as GST-fusion proteins in bacteria. Two fusion proteins of GST-AGS8-C, namely, AGS8-C1 (A^{1359}– H^{1493}) and AGS8-C2 (A^{1494} – T^{1585}), were successfully synthesized and migrated as expected on SDS-PAGE. While AGS8-C1 did not pull down purified Gβγ, AGS8-C2, which represented the FN3 domain, did pull down Gβγ, indicating the importance of the FN3 domain for the interaction of AGS8 with Gβγ (Fig. 1*D*).

AGS8-peptides Blocked the Interaction of AGS8C with Gβγ

To further determine the region of interaction between AGS8 and Gβγ, we prepared multiple 29- to 30-amino–acid peptides, the sequences of which were based on the amino acids from A^{1494} to W^{1730} of the rat AGS8 (ABB82299) (Fig. 2*A*). In a screen of 11 peptides by the GST-pull–down assay, which covered the entire region from A^{1494} to W^{1730} of the rat AGS8, we found two peptides, CP1 (A^{1494}PRNITVVAMEGCHSFVIVDWN-KAIPGDV^{1522}) and CP9 (S^{1508}FVIVDWNKAIPGDVVTGYL-VYSASYEDFI^{1537}) that effectively blocked the interaction of AGS8 with Gβγ in a dose-dependent manner (Fig. 2*B*). Quantitative analysis of immunoblots confirmed the dependence of the interaction of AGS8 with Gβγ on dose (Fig. 2*C*) and indicated that both peptides had similar IC50s (CP1:6.73×10^{-6} M; CP9:2.77×10^{-6} M). We first focused on CP9 and used this peptide as the AGS8-peptide in the following experiments.

The Gβγ-interaction Site of AGS8 was Localized at the FN3 Domain of the C-terminus of AGS8

The present data suggested that the first 45 amino acids of the FN3 domain represented by CP1 and CP2 were critical for AGS8 to interact with Gβγ and mediate signal to downstream molecules. The importance of this region for AGS8-mediated signaling was further examined in the yeast cells in which growth was linked to G-protein activation [23]. A deletion mutant of AGS8-C, which lacked the first 45 amino acids of this domain, failed to activate G-protein signaling, indicating the importance of this region for mediating AGS8-Gβγ signaling in the cell (Fig. 3).

The AGS8-peptide Inhibited Hypoxia-induced Internalization of Connexin 43 in Cardiomyocytes

In a previous study, we demonstrated that AGS8 was required for hypoxia-induced apoptosis of cardiomyocytes, which was associated with changes in the permeability of CX43 [13]. AGS8-Gβγ accelerates the internalization and degradation of channel

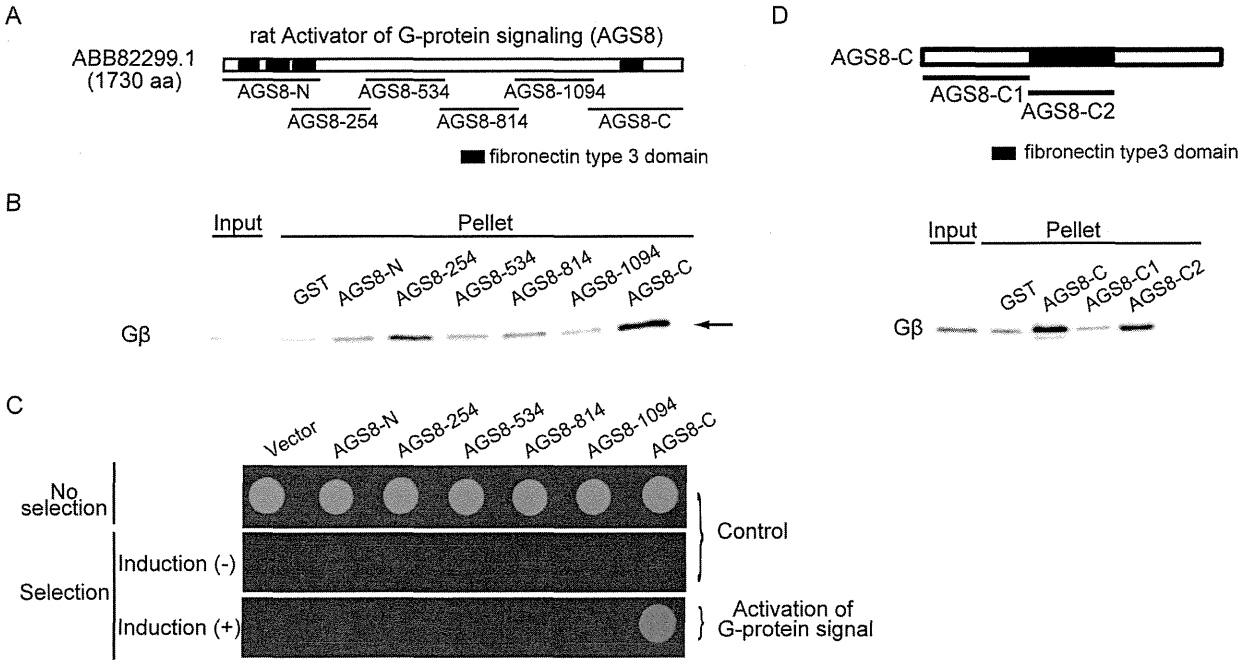

Figure 1. Determination of Gβγ interacting domain of the AGS8. (A) Schematic diagram of rat AGS8 and the AGS8 domains synthesized as GST-fusion proteins. Each GST protein fused with the following segment of rat AGS8 (ABB82299) respectively. AGS8-N: M^{1}- P^{370}, AGS8-254: A^{254}– R^{553}, AGS8-534: S^{534}– S^{833}, AGS8-814: S^{814}– R^{1113}, AGS8-1094: H^{1094}– D^{3280}, AGS8-C: A^{1359}– W^{1730}. (B) GST-pulldown assay of AGS8 domains with $G\beta_1\gamma_2$. AGS8 domains synthesized as GST-fusion proteins (300 nM) were incubated with recombinant human $G\beta_1\gamma_2$ (30 nM) in a total volume of 300 μl at 4°C. Proteins were then adsorbed to a glutathione matrix and retained G-protein subunits identified by immunoblotting following gel electrophoresis. The representative of 5 independent experiments with similar results. (C) Bioactivity of AGS8 domains on G-protein activation in cell. The yeast strain expressing human Gαs was transformed with AGS8 domains described in (A) into the pYES2-containing GAL1 promoter. The yeast strain was modified to grow without histidine on activation of G-protein. Induction(+): induction of translation of AGS8 domains by galactose. The representative of 4 independent experiments with similar results. (D) GST-pull down assay of AGS8-C segments with recombinant Gβγ. (*upper panel*) Schematic diagram of AGS8-C and the segments synthesized as GST-fusion proteins. Each GST protein fused with the following segment of rat AGS8 (ABB82299) respectively. AGS8-C1: A^{1359}– H^{1493}, AGS8-C2: A^{1494}– T^{1585}. (*lower panel*) GST-pulldown assay of AGS8 segments with $G\beta_1\gamma_2$. AGS8 domains synthesized as GST-fusion proteins (300 nM) were incubated with recombinant human $G\beta_1\gamma_2$ (30 nM) in a total volume of 300 μl at 4°C. Proteins were then adsorbed to a glutathione matrix and retained G-protein subunits identified by immunoblotting following gel electrophoresis. The representative of 4 independent experiments with similar results.
doi:10.1371/journal.pone.0091980.g001

protein CX43 under hypoxia, which results in decreased membrane permeability in the cardiomyocytes [13]. The change in localization and permeability of CX43 in the membrane is associated with hypoxia-induced apoptosis of the cardiomyocytes [14–16]. Therefore, we transferred the AGS8-peptide to cardiomyocytes and examined its effect on the internalization of CX43 induced by repetitive hypoxia (Fig. 4*A*).

The peptide was delivered to the cardiomyocytes by chemical reagent as described in "experimental procedures". Treatment of the cells with the chemical reagent and FITC-conjugated AGS8-peptide showed that the peptide was successfully delivered into the cardiomyocytes (Fig. 4*B*). The effect of the AGS8-peptide on internalization of CX43 was determined in the cardiomyocytes after hypoxic stress. CX43 was observed on the surface of the cardiomyocytes under normoxia (Fig. 4*B*), and its presence was decreased after exposure of the cardiomyocytes to repetitive hypoxia in the untransfected control cells and the cells exposed to transfection reagent alone (Fig. 4*B, 4C*). However, the AGS8-peptide dramatically blocked the internalization and degradation of CX43 induced by repetitive hypoxia (Fig. 4*B, 4C*). When the effect of FITC-conjugated AGS8-peptide was examined, FITC was observed in the cardiomyocytes under normoxia as well as hypoxia, and the hypoxia-induced internalization of CX43 was inhibited in FITC-positive cells (Fig. 4*B*).

The AGS8-peptide Inhibited the Decrease in Permeability of Connexin 43 Under Hypoxia

Loss of CX43 from the cell surface decreases influx and efflux of small molecules passing through CX43, and this effect is associated with apoptosis of the cardiomyocytes under hypoxia [13–16]. We next examined the ability of AGS8-peptide to block the change in permeability of CX43 by analyzing by the flux of the fluorescent dye, Lucifer Yellow (LY), which passes through CX43 as previously demonstrated [13]. LY in the culture medium was incorporated into cardiomyocytes under normoxia. The flux of dye was decreased after exposure of the cells to repetitive hypoxia in the control group as well as in the group exposed to transfection reagent alone (31.1±4.4%, 26.9±13.0%, respectively) (Fig. 5). However, the AGS8-peptide blocked the hypoxia-induced decrease in permeability in a dose-dependent manner. This observation is consistent with the immunofluorescence studies, in which CX43 was observed to remain at the cell surface after repetitive hypoxia in the presence of AGS8-peptide (Fig. 4).

The AGS8-peptide Protected Cardiomyocytes from Hypoxia-induced Apoptosis

To examine the effect of AGS8 peptide on apoptosis of the cardiomyocytes, cultured cardiomyocytes were sequentially ex-

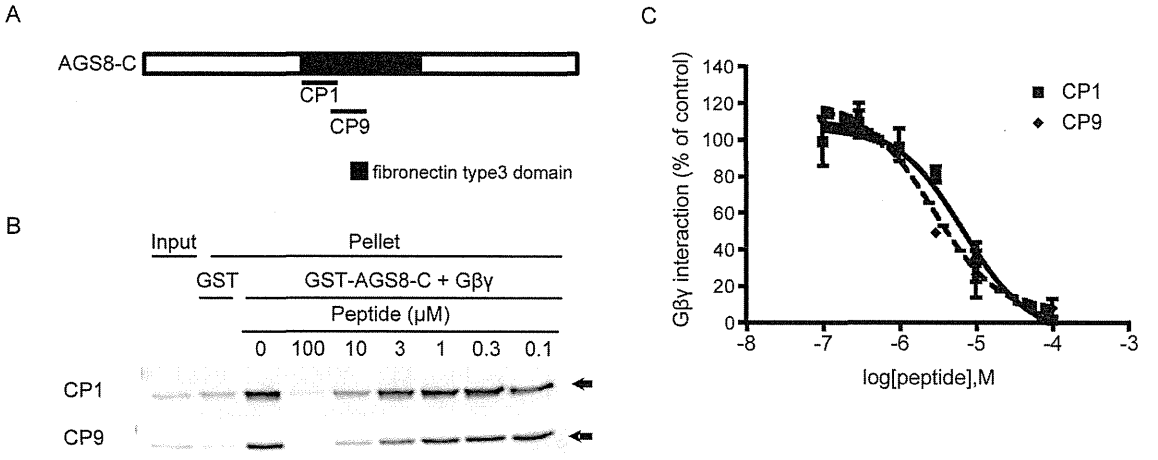

Figure 2. Development of AGS8 peptide. (A) Schematic diagram of AGS8-C and the AGS8-peptides (CP1 and CP9) which inhibited AGS8-Gβγ interaction. The AGS8-peptides were developed based on amino acid sequences of the Gβγ interaction domain of AGS8. CP1 and CP2 represented A^{1494}– V^{1522} and S^{1508}– I^{1537} of rat AGS8 (ABB82299) respectively. (B) The example of GST-pulldown assay of GST-AGS8-C with $G\beta_1\gamma_2$. GST-fusion protein (100 nM) was incubated with recombinant human $G\beta_1\gamma_2$ (10 nM) in the presence of AGS8-peptides (CP1 or CP9). Proteins were then adsorbed to a glutathione matrix and retained G-protein subunits identified by immunoblotting following gel electrophoresis. The representative of 6 independent experiments with similar results. (C) The densitometric analysis of GST-pulldown assay of GST-AGS8-C with $G\beta_1\gamma_2$ in the presence of AGS8-peptides. n = 6 with peptides of ~97% HPLC purity.
doi:10.1371/journal.pone.0091980.g002

posed to 1% oxygen for 6 h, then to 12 h of normoxia to induce hypoxia-mediated cell death (Fig. 6*A*) [13]. Hypoxia/reoxygenation markedly increased the number of apoptotic cardiomyocytes, as determined by TUNEL or immunostaining of cleaved caspase-3, in the untransfected control cells and those exposed to transfection reagent alone (Fig. 6B and 6C). However, AGS8-peptide successfully inhibited hypoxia-induced apoptosis, indicating a protective effect in cardiomyocytes. Additionally, the data indicated that, under normoxia, the AGS8-peptide did not influence apoptosis or the permeability of CX43 (Fig. 6*B and 6C*).

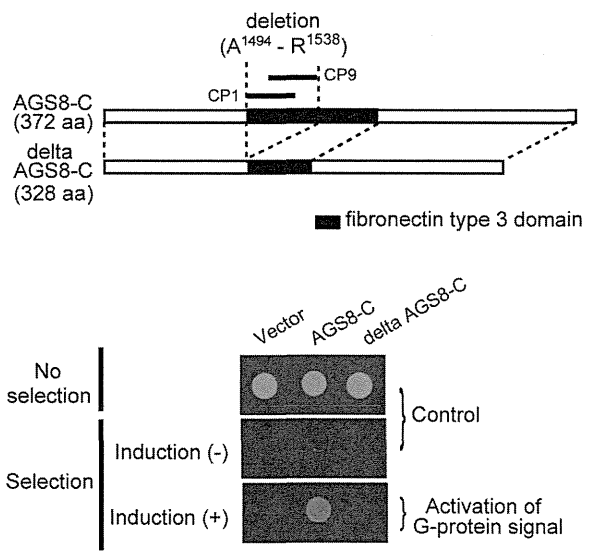

Figure 3. Effect of deletion of 45 amino acids of fibronectin type 3 domain. (A) Schematic diagram of C-terminal of AGS8 (AGS8-C) and the deleted mutant of AGS8-C (delta AGS8-C) lacking the first 45 amino acids of fibronectin type 3 domain, that are A^{1494} to R^{1538} of rat AGS8 (ABB82299). (B) Bioactivity of AGS8C and delta AGS8C on G-protein activation. The yeast strain expressing human Gαs was transformed with AGS8-C and delta AGS8-C in the pYES2-containing GAL1 promoter. The yeast strain was modified to grow without histidine on activation of G-protein. Induction (+): induction of translation of AGS8 domains by galactose. The representative of 4 independent experiments with similar results.
doi:10.1371/journal.pone.0091980.g003

Advantage of the AGS8-peptide for Targeted Disruption of the Gβγ Pathway

The data presented thus far indicated that the AGS8-peptide blocked the AGS8-Gβγ interaction and the signaling events the downstream of AGS8-Gβγ. We next asked whether inhibition of the Gβγ-mediated signal generally had a cardioprotective effect as was observed with the AGS8-peptide. Gallein is an inhibitor of Gβγ-mediated signaling that occupies a "common" interaction surface of Gβγ and inhibits the interaction of Gβγ-regulated proteins with Gβγ [25]. Thus, gallein is expected to block a wide range of Gβγ signals in cells, including CX43 regulation mediated by AGS-Gβγ. We previously demonstrated that gallein completely inhibits hypoxia-induced internalization of CX43 at 100 μM, as observed in the knockdown of AGS8, but not at 1 μM [13].

Here, we first examined the influence of the AGS8-peptide and gallein on the viability of cells. Cardiomyocytes were incubated with gallein for 24 h, and their viability was determined by MTT assay. Even the lowest concentration of gallein (1 μM) caused damage in the cardiomyocytes, indicating that broad inhibition of Gβγ did not have a protective effect (Fig. 7). In contrast, the AGS8-pepetide did not show cytotoxicity at 1 μM, the concentration that completely blocked the AGS8-Gβγ–mediated signal event. This suggests that the AGS8-peptide is a promising candidate for protection of cardiomyocytes from hypoxia-mediated apoptosis.

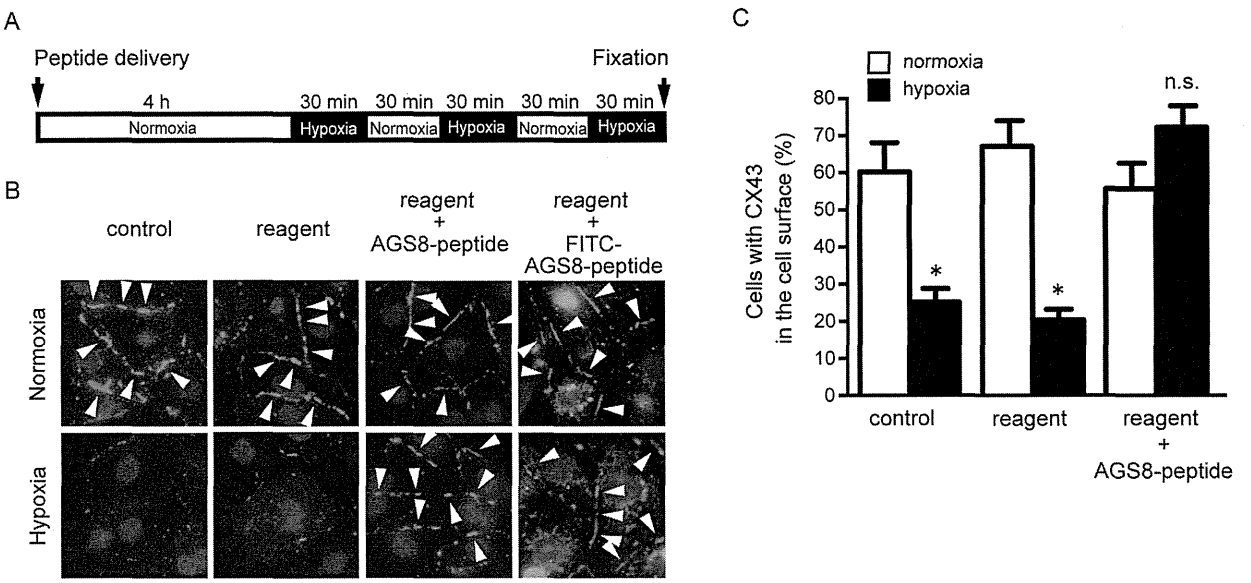

Figure 4. Effect of AGS8-peptide on localization of connexin 43 (CX43) of cultured cardiomyocytes. (A) *Cardiomyocytes were exposed* 3 times to 30 min of hypoxia (1% oxygen) intermittent with 30 min of reoxygenation 4 h after (without or with) transfection of AGS8-peptide (1 μM) or FITC-conjugated AGS8-peptide (1 μM). (B) Localization of CX43 in the cardiomyocytes under normoxia and hypoxia. The figures demonstrated in the triple color of CX43 (*red, arrow*), nuclei (DAPI, *blue*) and FITC-conjugated AGS8-peptide (*green*). The representative of 5 independent experiments with similar results. (C) The number of cardiomyocytes expressing CX43 in the cell surface were counted. Please note that ~ 90% cells were detectable at the point of fixation. Data are represent 170–260 cells from 5 of independent experiments. *, $p<0.05$ vs normoxia group.
doi:10.1371/journal.pone.0091980.g004

Discussion

AGS8-peptide, the sequence of which was derived from the amino-acid sequences of the Gβγ-binding domain of AGS8, blocked the association of AGS8 with Gβγ and inhibited AGS8-mediated events under hypoxia. Notably, AGS8-peptide inhibited the change in permeability of cell-surface CX43 and the apoptosis of cardiomyocytes. AGS8-peptide did not show cytotoxicity under normoxia, in contrast to the small molecule gallein, which produced deleterious effects by general inhibition of Gβγ-signaling. These data indicate that the AGS8-Gβγ complex plays a pivotal role in triggering the hypoxia-induced apoptosis of cardiomyocytes. Furthermore, they suggest an advantage of targeted disruption of G-protein signaling by the AGS-based peptide in protecting cardiomyocytes from hypoxia-induced apoptosis.

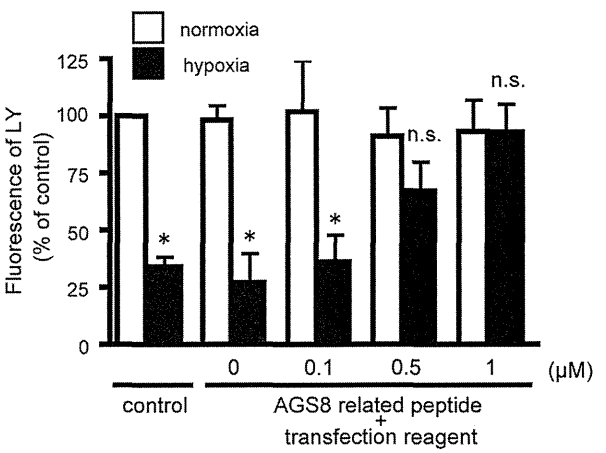

Figure 5. Uptake of connexin selective fluorescence dye, Lucifer Yellow (LY) to the cardiomyocytes. Cells were incubated with 1 mM of LY for 45 min in normal culture medium. Excess LY was removed and cells were rinsed with PBS. The fluorescence of LY was evaluated by inverted fluorescence microscope. The fluorescence of LY was quantified by the intensity of fluorescence of 10 randomly selected fields. The non-selective binding and/or incorporation of LY was determined fluorescence in the presence of a connexin hemichannel blocker, 50 μM of Lanthanum which was added 30 min prior to LY. *, $p<0.05$ vs cells in normoxia; *n.s.*, not statistically significant. N = 4 from 4 independent experiments.
doi:10.1371/journal.pone.0091980.g005

Several peptides have been developed to manipulate the broad signal initiated by accessory proteins for G-proteins. For example, an inhibitor of accessory proteins for heterotrimeric G-protein has been developed for RGS proteins. RGS proteins share 120–130 amino acids of an RGS-homology domain, which interact with the Gα subunit and accelerate GTPase activity [26,27]. RGS-peptides, which were designed on the basis of the X-ray structure of the Gαi switch I region of RGS4-Gαi, successfully modulate muscarinic receptor-regulated potassium currents in atrial myocytes [28]. RGS-peptides were initially designed to mimic the surface of G-protein to inhibit GAP activity, which produced the potential to suppress many events mediated by a variety of RGS proteins. As another example, a peptide, the sequence of which is based on G-protein regulatory (GPR) or GoLOCO motifs, is a cassette of 20–25 amino acids that stabilizes the GDP-bound conformation of Gα and clearly inhibits Gαi activation in vitro, suggesting its potential as an inhibitor of general Gαi signaling in cells [29].

Alternatively, the AGS8 peptide was designed on the basis of the AGS-Gβγ interface, with the objective of suppressing the specific signal evoked by AGS-Gβγ for all Gβγ signaling. It has been demonstrated that Gβγ-interacting proteins share an overlapping

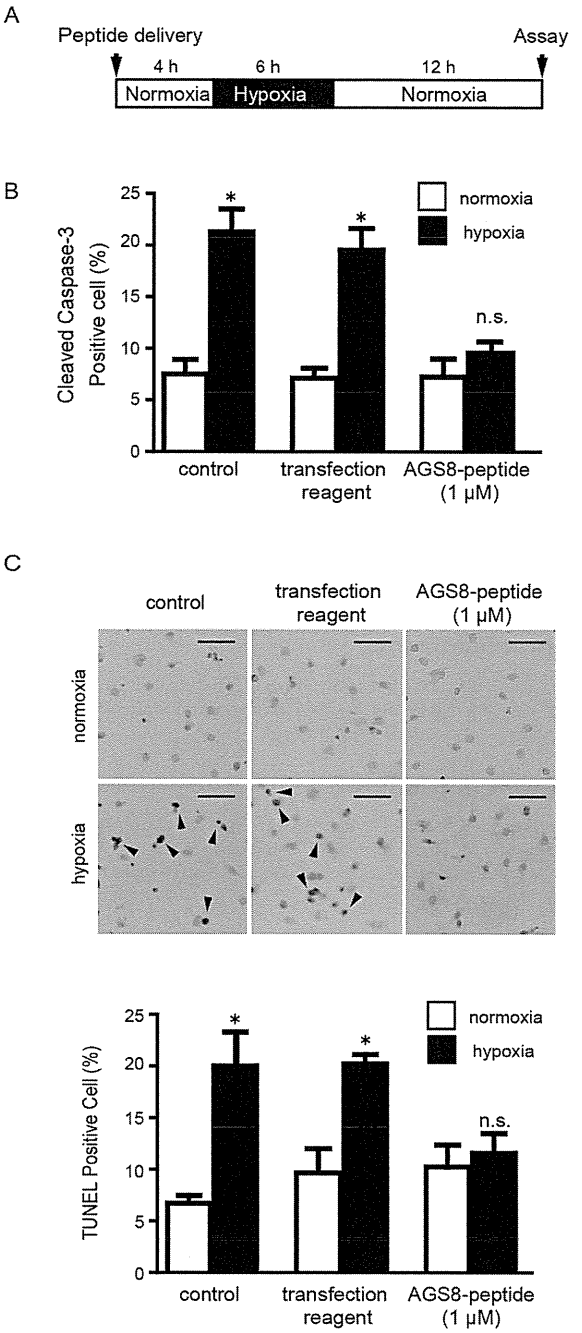

Figure 6. Effect of AGS8 peptide on hypoxia-induced apoptosis of cardiomyocytes. (A) Neonatal cardiomyocytes were exposed to hypoxia (1% oxygen) or normoxia as indicated duration without or with introduction of AGS8-peptide. Apoptosis was assessed by immunofluorescent detection of the active form of caspase-3 (cleaved caspase-3) (B) or TUNEL stain (C) as described in the experimental procedures. (C) Upper panel indicates representative apoptotic (*dark blue, arrow*) and non-apoptotic cells (*red*) after TUNEL staining. Scale bars indicate 100 μm. Approximately 3000 cells of 10 independent fields were counted for each experiments. A separate experiment indicated that AGS8-peptide did not influence the level of AGS8 within the 4-h treatment (1.0 μM peptide; 98.2±7.3% versus no reagent alone group, not statistically significant, $n = 4$). *, $p<0.05$ vs cells in normoxia; *n.s.*, not statistically significant. N = 5 from 5 independent experiments.
doi:10.1371/journal.pone.0091980.g006

interface on the surface of Gβγ [30,31]. We previously demonstrated that the Gβγ-interacting surface of AGS8 includes the shared-site [32]. However, the entire Gβγ-interacting surface of AGS8 may include an additional interface, which is required to form an AGS8-specific signal complex. Our results indicated that 45 amino acids were required to evoke cell signaling by the AGS-Gβγ complex. The amino acid sequence of this domain did not have similarity to other known Gβγ interfaces [33–35], suggesting this sequence represents the AGS8-specifc interface that forms this particular complex. In fact, the AGS8-peptide designed to recognize this region successfully inhibited formation of the AGS8-Gβγ complex and subsequent cell events mediated by AGS8-Gβγ. However, currently, there is not enough information to determine whether the AGS8-peptide covers the common Gβγ interface or influences the interaction of Gβγ with other molecules. These issues are to be investigated elsewhere.

AGS-Gβγ–mediated signaling is required for hypoxia-induced apoptosis of cardiomyocytes [13]. Gβγ is known to conduct pro-apoptotic signaling via p38MAPK, JNK, or PLCβ, whereas anti-apoptotic signaling is also mediated by Gβγ via PI3K-Akt or ERK depending on type of cell and stimulus [36–39]. Although the involvement of these Gβγ-mediated pathways in the AGS-Gβγ pathway or other players in the AGS-Gβγ protein complex are yet to be determined, the current data indicate the presence of a critical signaling pathway mediated by the AGS8-Gβγ complex leading to apoptosis in cardiomyocytes.

The channel protein CX43 plays a role in the apoptotic process by regulating the permeability of small molecules, including adenosine 5′-triphosphate, adenosine diphosphate, adenosine, cAMP, inositol-1,4,5-triphosphate, glutamate, and glutathione [14,15,40–42]. In response to hypoxia, AGS8 organizes the complex that includes Gβγ, CX43, and possibly kinases that initiate phosphorylation of CX43 [13]. Multiple phosphorylation sites on CX43 are regulated by specific kinases under ischemic

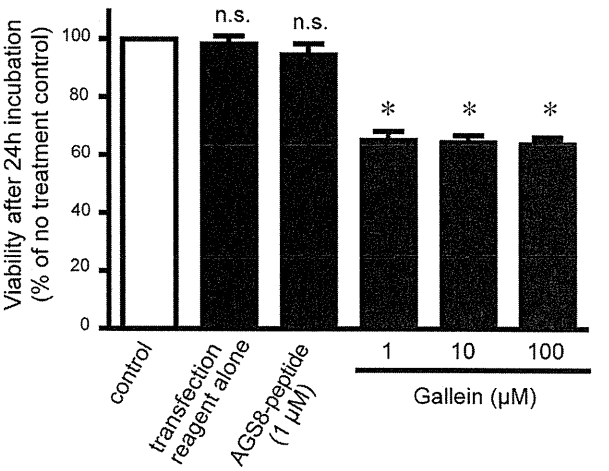

Figure 7. Effect of AGS8-peptide or Gallein on the viability of cardiomyocytes determined by MTT assay. Neonatal cardiomyocytes were cultured for 24 h with AGS8-peptide or Gallein. Gallein occupied a "common" interaction surface of Gβγ and inhibited its interaction with Gβγ-regulated proteins. *, $p<0.05$ vs cells in normoxia; *n.s.*, not statistically significant. N = 5 from 5 independent experiments.
doi:10.1371/journal.pone.0091980.g007

conditions, and each phosphorylation critically influences the permeability and localization of CX43 in the sarcolemma [43,44]. The inhibition of internalization of CX43 by AGS8-peptide may suggest that AGS8-peptide blocked the recruitment of components into the complex and/or phosphorylation of CX43 within the complex. AGS8 may play a role in separating the hypoxic/ischemic cardiomyocytes from healthy tissue by disconnecting the gap junction, which can contribute to arrhythmia and contraction failure during ischemia. Although the validity of this hypothesis is yet to be tested in confirmed or animal models, our observations support this possibility.

Myocardial ischemia activates multiple cascades that initiate intracellular ionic and chemical changes leading cell to death [17,18]. Although great efforts have been made over many years, therapeutic approaches to ischemic heart disease still need further development [45,46]. We previously demonstrated that AGS8-Gβγ signaling was activated under hypoxia and did not constitutively stimulate the apoptotic pathway, because the pro-apoptotic effects of AGS were not observed in cells cultured under normoxia [13]. In fact, AGS8-peptide effectively protected cardiomyocytes from hypoxia-mediated cell death, but did not cause cell damage under normoxia. Thus, AGS8-peptide has the potential to save a subpopulation of cardiomyocytes exposed to hypoxia without producing damage to the entire myocardium. This is an advantage of targeted disruption of specific signaling by AGS8-peptide, and it stands in contrast to the deleterious effects caused by general inhibition of Gβγ signaling with gallein.

Peptide-based reagents designed from the sequences of accessory proteins for heterotrimeric G-protein have potential to manipulate alternative signaling events distinct from GPCR-mediated G-protein signaling. At this stage, the potential of peptide-based reagents, including AGS8-peptide, remains limited by their ability to penetrate the membrane, their stability, and the modes of delivery available for their use as clinical drugs. The strategies for effective delivery of therapeutic peptides into the cell include conjugation with cell-penetrating peptides, incorporation into polymeric nanoparticles, and virus-mediated release of peptides [47–49]. Each strategy still has challenges with respect to the efficiency or selectivity of delivery as well as safety in healthy tissues or cells [47,49,50]. Although intracellular use of peptide targeting is not yet a common practice, delivery systems are continuously being developed, which will increase the potential for use of peptide-targeting therapy. We have demonstrated the possibility of regulating intracellular signaling mediated by accessory proteins for heterotrimeric G-protein, which could be a starting point for development of peptides or compounds to regulate AGS8-Gβγ signaling.

Targeted disruption of the interaction of G-protein with accessory proteins for heterotrimeric G-protein is a promising therapeutic strategy because these molecules mediate critical signaling distinct from the receptor-mediated pathway. In this study, we demonstrated that AGS8-peptide could be part of a novel therapeutic approach for the protection of ischemia in the heart that has enhanced specificity and fewer side effects. Although efforts to intervene in G-protein signaling have been focused on the interface of the GPCR-heterotrimeric G-protein, our data highlight the advantages of accessory proteins for heterotrimeric G-protein as alternative therapeutic targets in human diseases.

Acknowledgments

We acknowledge Dr. James R. Broach (Molecular Biology, Princeton University, NJ, USA) and Cadus Pharmaceutical Corp. (NY, USA) for providing yeast strains used in this study.

Author Contributions

Conceived and designed the experiments: M. Sato. Performed the experiments: M. Sato MH HS YY. Analyzed the data: M. Sakima AAM TF UY SO. Contributed reagents/materials/analysis tools: UY SO TF YI. Wrote the paper: M. Sato.

References

1. Birnbaumer L (2007) Expansion of signal transduction by G proteins. The second 15 years or so: from 3 to 16 alpha subunits plus betagamma dimers. Biochim Biophys Acta 1768: 772–793.
2. Sato M, Blumer JB, Simon V, Lanier SM (2006) ACCESSORY PROTEINS FOR G PROTEINS: Partners in Signaling. Annu Rev Pharmacol Toxicol 46: 151–187.
3. Blumer JB, Smrcka AV, Lanier SM (2007) Mechanistic pathways and biological roles for receptor-independent activators of G-protein signaling. Pharmacol Ther 113: 488–506.
4. Sjogren B (2011) Regulator of G protein signaling proteins as drug targets: current state and future possibilities. Adv Pharmacol 62: 315–347.
5. Sato M (2013) Roles of Accessory Proteins for Heterotrimeric G-Protein in the Development of Cardiovascular Diseases. Circ J.
6. Cismowski MJ, Ma C, Ribas C, Xie X, Spruyt M, et al. (2000) Activation of heterotrimeric G-protein signaling by a ras-related protein. Implications for signal integration. J Biol Chem 275: 23421–23424.
7. McGrath MF, Ogawa T, de Bold AJ (2012) Ras dexamethasone-induced protein 1 is a modulator of hormone secretion in the volume overloaded heart. Am J Physiol Heart Circ Physiol 302: H1826–1837.
8. Wieland T, Mittmann C (2003) Regulators of G-protein signalling: multifunctional proteins with impact on signalling in the cardiovascular system. Pharmacol Ther 97: 95–115.
9. Gu S, Cifelli C, Wang S, Heximer SP (2009) RGS proteins: identifying new GAPs in the understanding of blood pressure regulation and cardiovascular function. Clin Sci (Lond) 116: 391–399.
10. Zhang P, Mende U (2011) Regulators of G-protein signaling in the heart and their potential as therapeutic targets. Circ Res 109: 320–333.
11. Sato M, Hiraoka M, Suzuki H, Bai Y, Kurotani R, et al. (2011) Identification of transcription factor E3 (TFE3) as a receptor-independent activator of Galpha16: gene regulation by nuclear Galpha subunit and its activator. J Biol Chem 286: 17766–17776.
12. Sato M, Cismowski MJ, Toyota E, Smrcka AV, Lucchesi PA, et al. (2006) Identification of a receptor-independent activator of G protein signaling (AGS8) in ischemic heart and its interaction with Gbetagamma. Proc Natl Acad Sci U S A 103: 797–802.
13. Sato M, Jiao Q, Honda T, Kurotani R, Toyota E, et al. (2009) Activator of G protein signaling 8 (AGS8) is required for hypoxia-induced apoptosis of cardiomyocytes: role of G betagamma and connexin 43 (CX43). J Biol Chem 284: 31431–31440.
14. Harris AL (2007) Connexin channel permeability to cytoplasmic molecules. Prog Biophys Mol Biol 94: 120–143.
15. Rodriguez-Sinovas A, Cabestrero A, Lopez D, Torre I, Morente M, et al. (2007) The modulatory effects of connexin 43 on cell death/survival beyond cell coupling. Prog Biophys Mol Biol 94: 219–232.
16. Zhang SS, Shaw RM (2013) Multilayered regulation of cardiac ion channels. Biochim Biophys Acta 1833: 876–885.
17. Yellon DM, Hausenloy DJ (2007) Myocardial reperfusion injury. N Engl J Med 357: 1121–1135.
18. Bishopric NH, Andreka P, Slepak T, Webster KA (2001) Molecular mechanisms of apoptosis in the cardiac myocyte. Curr Opin Pharmacol 1: 141–150.
19. Sato M, Gettys TW, Lanier SM (2004) AGS3 and signal integration by Galpha(s)- and Galpha(i)-coupled receptors: AGS3 blocks the sensitization of adenylyl cyclase following prolonged stimulation of a Galpha(i)-coupled receptor by influencing processing of Galpha(i). J Biol Chem 279: 13375–13382.
20. Sato M, Ribas C, Hildebrandt JD, Lanier SM (1996) Characterization of a G-protein activator in the neuroblastoma-glioma cell hybrid NG108-15. J Biol Chem 271: 30052–30060.
21. Sato M, Ohsaki Y, Tobise K (1995) Transforming growth factor-beta 1 proliferated vascular smooth muscle cells from spontaneously hypertensive rats. Am J Hypertens 8: 160–166.
22. Thuc LC, Teshima Y, Takahashi N, Nagano-Torigoe Y, Ezaki K, et al. (2010) Mitochondrial K(ATP) channels-derived reactive oxygen species activate pro-survival pathway in pravastatin-induced cardioprotection. Apoptosis 15: 669–678.
23. Cismowski MJ, Takesono A, Ma C, Lizano JS, Xie X, et al. (1999) Genetic screens in yeast to identify mammalian nonreceptor modulators of G-protein signaling. Nat Biotechnol 17: 878–883.
24. Takesono A, Cismowski MJ, Ribas C, Bernard M, Chung P, et al. (1999) Receptor-independent activators of heterotrimeric G-protein signaling pathways. J Biol Chem 274: 33202–33205.

25. Lehmann DM, Seneviratne AM, Smrcka AV (2008) Small molecule disruption of G protein beta gamma subunit signaling inhibits neutrophil chemotaxis and inflammation. Mol Pharmacol 73: 410–418.
26. Sjogren B, Blazer LL, Neubig RR (2010) Regulators of G protein signaling proteins as targets for drug discovery. Prog Mol Biol Transl Sci 91: 81–119.
27. Kimple AJ, Bosch DE, Giguere PM, Siderovski DP (2011) Regulators of G-protein signaling and their Galpha substrates: promises and challenges in their use as drug discovery targets. Pharmacol Rev 63: 728–749.
28. Roof RA, Jin Y, Roman DL, Sunahara RK, Ishii M, et al. (2006) Mechanism of action and structural requirements of constrained peptide inhibitors of RGS proteins. Chem Biol Drug Des 67: 266–274.
29. Peterson YK, Bernard ML, Ma H, Hazard S 3rd, Graber SG, et al. (2000) Stabilization of the GDP-bound conformation of Gialpha by a peptide derived from the G-protein regulatory motif of AGS3. J Biol Chem 275: 33193–33196.
30. Ford CE, Skiba NP, Bae H, Daaka Y, Reuveny E, et al. (1998) Molecular basis for interactions of G protein betagamma subunits with effectors. Science 280: 1271–1274.
31. Smrcka AV (2008) G protein betagamma subunits: Central mediators of G protein-coupled receptor signaling. Cell Mol Life Sci 65: 2191–2214.
32. Yuan C, Sato M, Lanier SM, Smrcka AV (2007) Signaling by a non-dissociated complex of G Protein betagamma and alpha subunits stimulated by a receptor-independent activator of G protein signaling, AGS8. J Biol Chem 282: 19938–19947.
33. Touhara K, Inglese J, Pitcher JA, Shaw G, Lefkowitz RJ (1994) Binding of G protein beta gamma-subunits to pleckstrin homology domains. J Biol Chem 269: 10217–10220.
34. Chen J, DeVivo M, Dingus J, Harry A, Li J, et al. (1995) A region of adenylyl cyclase 2 critical for regulation by G protein beta gamma subunits. Science 268: 1166–1169.
35. Qin N, Platano D, Olcese R, Stefani E, Birnbaumer L (1997) Direct interaction of gbetagamma with a C-terminal gbetagamma-binding domain of the Ca2+ channel alpha1 subunit is responsible for channel inhibition by G protein-coupled receptors. Proc Natl Acad Sci U S A 94: 8866–8871.
36. New DC, Wu K, Kwok AW, Wong YH (2007) G protein-coupled receptor-induced Akt activity in cellular proliferation and apoptosis. FEBS J 274: 6025–6036.
37. Goldsmith ZG, Dhanasekaran DN (2007) G protein regulation of MAPK networks. Oncogene 26: 3122–3142.
38. Marinissen MJ, Gutkind JS (2001) G-protein-coupled receptors and signaling networks: emerging paradigms. Trends Pharmacol Sci 22: 368–376.
39. Adams JW, Brown JH (2001) G-proteins in growth and apoptosis: lessons from the heart. Oncogene 20: 1626–1634.
40. Shintani-Ishida K, Uemura K, Yoshida K (2007) Hemichannels in cardiomyocytes open transiently during ischemia and contribute to reperfusion injury following brief ischemia. Am J Physiol Heart Circ Physiol 293: H1714–1720.
41. Solan JL, Marquez-Rosado L, Sorgen PL, Thornton PJ, Gafken PR, et al. (2007) Phosphorylation at S365 is a gatekeeper event that changes the structure of Cx43 and prevents down-regulation by PKC. J Cell Biol 179: 1301–1309.
42. Bao X, Lee SC, Reuss L, Altenberg GA (2007) Change in permeant size selectivity by phosphorylation of connexin 43 gap-junctional hemichannels by PKC. Proc Natl Acad Sci U S A 104: 4919–4924.
43. Ek-Vitorin JF, King TJ, Heyman NS, Lampe PD, Burt JM (2006) Selectivity of connexin 43 channels is regulated through protein kinase C-dependent phosphorylation. Circ Res 98: 1498–1505.
44. Lampe PD, Cooper CD, King TJ, Burt JM (2006) Analysis of Connexin43 phosphorylated at S325, S328 and S330 in normoxic and ischemic heart. J Cell Sci 119: 3435–3442.
45. Windecker S, Bax JJ, Myat A, Stone GW, Marber MS (2013) Future treatment strategies in ST-segment elevation myocardial infarction. Lancet 382: 644–657.
46. Jneid H (2012) The 2012 ACCF/AHA Focused Update of the Unstable Angina/Non-ST-Elevation Myocardial Infarction (UA/NSTEMI) Guideline: a critical appraisal. Methodist Debakey Cardiovasc J 8: 26–30.
47. Clemons TD, Viola HM, House MJ, Iyer KS, Hool LC (2013) Examining efficacy of "TAT-less" delivery of a peptide against the L-type calcium channel in cardiac ischemia-reperfusion injury. ACS Nano 7: 2212–2220.
48. Flores-Munoz M, Godinho BM, Almalik A, Nicklin SA (2012) Adenoviral delivery of angiotensin-(1–7) or angiotensin-(1–9) inhibits cardiomyocyte hypertrophy via the mas or angiotensin type 2 receptor. PLoS One 7: e45564.
49. Svensen N, Walton JG, Bradley M (2012) Peptides for cell-selective drug delivery. Trends Pharmacol Sci 33: 186–192.
50. Jones AT, Sayers EJ (2012) Cell entry of cell penetrating peptides: tales of tails wagging dogs. J Control Release 161: 582–591.

J Physiol Sci (2014) 64:177–183
DOI 10.1007/s12576-014-0309-8

ORIGINAL PAPER

Hyperthermia generated with ferucarbotran (Resovist®) in an alternating magnetic field enhances cisplatin-induced apoptosis of cultured human oral cancer cells

Itaru Sato · Masanari Umemura · Kenji Mitsudo · Mitomu Kioi · Hideyuki Nakashima · Toshinori Iwai · Xianfeng Feng · Kayoko Oda · Akiyoshi Miyajima · Ayako Makino · Maki Iwai · Takayuki Fujita · Utako Yokoyama · Satoshi Okumura · Motohiko Sato · Haruki Eguchi · Iwai Tohnai · Yoshihiro Ishikawa

Received: 27 January 2014 / Accepted: 20 February 2014 / Published online: 12 March 2014

Abstract Hyperthermia is a promising anti-cancer treatment in which the tissue temperature is increased to 42–45 °C, and which is often used in combination with chemotherapy or radiation therapy. Our aim in the present work was to examine the feasibility of combination therapy for oral cancer with cisplatin and hyperthermia generated with ferucarbotran (Resovist®; superparamagnetic iron oxide) in an alternating magnetic field (AMF). First, we established that administration of ferucarbotran at the approved dosage for magnetic resonance imaging provides an iron concentration sufficient to increase the temperature to 42.5 °C upon exposure to AMF. Then, we examined the effect of cisplatin combined with ferucarbotran/AMF-induced hyperthermia on cultured human oral cancer cells (HSC-3 and OSC-19). Cisplatin alone induced apoptosis of cancer cells in a dose-dependent manner, as is well known. However, the combination of cisplatin with ferucarbotran/AMF was significantly more effective than cisplatin alone. This result suggests that it might be possible to reduce the clinically effective dosage of cisplatin by administering it in combination with ferucarbotran/AMF-induced hyperthermia, thereby potentially reducing the incidence of serious cisplatin-related side effects. Further work seems justified to evaluate simultaneous thermo-chemotherapy as a new approach to anticancer therapy.

Keywords Ferucarbotran · Hyperthermia · Oral cancer · Anti-cancer effect · Cisplatin · Resovist®

Abbreviations

AMF	Alternating magnetic field
MNPs	Magnetic nanoparticles
MRI	Magnetic resonance imaging
SPIO	Superparamagnetic iron oxide

Introduction

Cancer cells are more vulnerable to increased temperature than normal cells [1]. Thus, hyperthermia is viewed as a promising approach in cancer therapy [2]. Many techniques have been reported to increase the temperature of cancer tissues, such as whole-body hyperthermia [3], radiofrequency hyperthermia [4], microwave-induced hyperthermia [5], and implantable needles [6]. However, with all

I. Sato · M. Umemura (✉) · X. Feng · K. Oda · A. Miyajima · A. Makino · M. Iwai · T. Fujita · U. Yokoyama · Y. Ishikawa (✉)
Cardiovascular Research Institute, Yokohama City University, Graduate School of Medicine, 3-9 Fukuura, Yokohama 236-0004, Japan
e-mail: umemurma@yokohama-cu.ac.jp

Y. Ishikawa
e-mail: yishikaw@med.yokohama-cu.ac.jp

I. Sato · K. Mitsudo · M. Kioi · H. Nakashima · T. Iwai · I. Tohnai
Department of Oral and Maxillofacial Surgery, Yokohama City University Graduate School of Medicine, 3-9 Fukuura, Yokohama 236-0004, Japan

S. Okumura
Tsurumi University School of Dental Medicine, Tsurumi 230-8501, Japan

M. Sato
Department of Physiology, Aichi Medical University, Nagakute 480-1195, Aichi, Japan

H. Eguchi
Advanced Applied Science Department, Research Laboratory, IHI Corporation, Yokohama 235-8501, Japan